Analysis of the THAI Iod-11 and Iod-12 tests: advancements and limitations of ASTEC V2.0R3p1 and MELCOR V2.1.4803

Corresponding author:
Bruno Gonfiotti – University of Pisa, Dipartimento di Ingegneria Civile e Industriale, Largo Luciano Lazzarino 1, 56126, Pisa, Italy. Mail: bruno.gonfiotti@for.unipi.it. Mobile: (+39) 333 1716086

Co-author:
Sandro Paci –University of Pisa, Dipartimento di Ingegneria Civile e Industriale, Largo Luciano Lazzarino 1, 56126, Pisa, Italy. Mail: s.paci@unipi.it

Abstract

This work is related to the application of the ASTEC V2.0R3p1 and MELCOR V2.1.4803 codes to the analysis of the THAI Iod-11 and Iod-12 containment tests characterized by an iodine release. The main scope of these two tests was to investigate the iodine-steel interaction on dry and wet surfaces, with an interaction supposed to be a two-steps process: an initial faster and reversible physisorption followed by a slower, and irreversible, chemisorption of the physisorbed I_2. The aim of the present work is to highlight advancements and limitations of the current ASTEC and MELCOR code versions respect to the older code versions employed during the European SARNET projects. The investigation was carried out as a code-to-code comparison vs. the experimental THAI data, focusing on the evaluation of the code models treating the iodine behaviour. A similar spatial nodalisation was employed for both codes. As main result, ASTEC had shown an overall good agreement compared to the iodine related experimental data while, on contrary, MELCOR had shown poor results, probably due to unsolved numerical issues and unsatisfactory iodine modellisation.

Keywords

THAI, Iod-11 test, Iod-12 test, iodine behaviour, ASTEC, MELCOR.

Abbreviations:
AECL: Atomic Energy of Canada Limited; **CSNI:** Committee on the Safety of Nuclear Installations; **FPC**: Fission Product Chemistry; **EU**: European Union; **GRS:** Gesellschaft für Anlagen- und Reaktorsicherheit; **IP:** Iodine Pool; **IRSN:** Institut de Radioprotection et de Sûreté Nucléaire; **NPP:** Nuclear Power Plant; **r.h.:** Relative Humidity; **SA**: Severe Accident; **SARNET:** Severe Accident Research NETwork of excellence**; THAI**: Thermal-hydraulic, Hydrogen, Aerosol and Iodine.

1 Introduction

Iodine is one of the major contributors to the external source term during a SA[1] for its volatility and high radiological consequences. Therefore, large efforts have been carried out [1] to describe the iodine behaviour during an accident within the nuclear island of a NPP[2], especially in the containment system. In many cases a well-mixed containment atmosphere is assumed during the source term analysis, but the presence of hydrogen and aerosols can lead to stratified atmosphere conditions. These different atmospheric conditions respect to the well-mixed assumption can influence iodine local concentrations, and thus its behaviour in the various containment zones. The iodine concentration influences its reaction rates, therefore a proper evaluation of the local concentrations should be accurate, especially for I_2, which is highly volatile. Other main thermal-hydraulics parameters influencing the iodine reaction rates are the local temperatures and humidity, the wall condensation rate, and the wall surface temperatures. Therefore the iodine source term is highly influenced by containment thermal-hydraulics conditions. Several SA codes have an integrated containment iodine model, like ASTEC/IODE, MAAP/IMPAR, etc. for the evaluation of its transport and the coupling of the iodine chemistry with thermal-hydraulics and aerosol physics. However, the validation of such coupling effects in the past was rather limited due to the scarce experimental data available. Moreover, the rough iodine models implemented in the various code lead to an unsatisfactory prediction of iodine behaviour, but in these last few years, many attempts were carried out to increase the experimental data available and then to refine its modeling.

As part of these efforts, models investigating iodine-steel interactions have been developed in the last years [1]. Early researches focused on a simple single step process, accounting for "*physisorption*" (physical deposition onto steel surfaces) and "*chemisorption*" (iodine reacts with steel forming FeI_2) at the same time [2]. On more recent year, a new approach characterized by a two-step process has been followed [3] accounting for a first, fast and reversible, "*physisorption*" followed by a slower and irreversible "*chemisorption*", where both reactions are influenced by the local wall-surface temperatures and relative humidity. This model, initially developed for ambient temperature and low relative humidity (<35%) [3] have been extended in the recent year to cope also with high temperatures and relative humilities [4]. However, as reported in the CSNI[3] Status Report on Iodine Behaviour [1], uncertainties on iodine sorption are still present and, in particular, the influence of temperature and relative humidity has not been established rigorously. Further AECL[4] studies have also highlighted that both the nature of the carrier gas and the rate of the mass transfer towards the steel surface influences the iodine sorption. The interpretation of new tests should fill these gaps [1] and for these reasons the THAI[5] Iod-11 and Iod-12 tests were carried out [4]. These two tests are characterized by a molecular iodine (I_2) release in a large and compartmented steel vessel with the scope to address iodine distribution inside the containment system under stratified and well-mixed conditions, differing each other for the wall condensation, avoided only in Iod-11.

These two tests were originally released in a benchmark [4] under the EU[6] SARNET[7] framework [5] in order to investigate the coupling between containment thermal-hydraulics and iodine codes, and

---

[1] Severe Accident
[2] Nuclear Power Plant
[3] Committee on the Safety of Nuclear Installations
[4] Atomic Energy of Canada Limited
[5] Thermal-hydraulic, Hydrogen, Aerosol and Iodine
[6] European Union
[7] Severe Accident Research NETwork of excellence

to evaluate the capability of the SA codes to simulate the iodine-steel interactions. At the end of this benchmark (2012) a report covering the main findings was issued [4], stating that the employed codes, common employed in SA studies, were able to simulate the two THAI tests but large discrepancies were also present, especially on thermal-hydraulics and in iodine modelling. For these reasons, model improvements and then further investigations were suggested.

Two of the main SA codes extensively employed during the SARNET framework were ASTEC and MELCOR [4]. The ASTEC code, joint developed by IRSN[8] and GRS[9], treats the iodine behaviour in the IODE module, which had yet received positive reviews during the analysis of other experimental tests, like Phébus-FP tests and previous THAI tests [6] [7] [8]. The MELCOR V2.1 code can treats iodine behaviour with three models: with a simple chemisorption model, with a more complex Iodine Pool (IP[10]) model or with the fission product chemistry (FPC[11]) model. The chemisorption model is not able to simulate the iodine resuspension phenomena, therefore it cannot be applied to the Iod-11 and Iod-12 tests. On contrary, the IP model can cope with resuspension, but in other previous applications large discrepancies have been shown on the final iodine mass balance .

The purpose of the present work can be easily subdivided in four parts:

- Re-evaluate the ThAI tests with the MELCOR and the ASTEC codes, because during the SARNET benchmark the University of Pisa provided results obtained with the ECART code [4].
- Employing an identical nodalisation in both codes to allow a comparison 1:1 among the capabilities of the two codes. In the SARNET exercise the comparison among different codes was not so stressed due to the different nodalisation employed by each participant [4].
- In the SARNET exercise only the older MELCOR 1.8.x versions were employed [4], while in this work only the new 2.1 version was employed.
- Provide a continuous validation of the SA codes against well-known tests. New features and bugs fixing were introduced in the latest ASTEC and MELCOR versions, thus is fundamental to demonstrate that the quality of the results obtained increases instead of decreases. Moreover, a high quality characterizes the data provided during the SARNET benchmark exercise reducing the needing of user's assumption, and hence the user's influence on the final results. For this purpose the two tests are very valuable to provide a continuous validation of the main SA codes.

The article is structured in eleven parts:

- The first part is a brief introduction of this paper;
- The second and the third parts describe the THAI facility and the THAI vessel respectively;
- The fourth and fifth parts describe the main phenomena characterizing the Iod-11 and Iod-12 tests;
- The sixth part describes the employed nodalisation in both the ASTEC and the MELCOR codes;
- The seventh part deeply describes the iodine-steel interaction, basing on the main literature documents;
- The eighth and the nineth parts describe the main results of the analyses carried out on both tests;

[8] Institut de Radioprotection et de Sûreté Nucléaire

[9] Gesellschaft für Anlagen- und Reaktorsicherheit

[10] Iodine Pool Model

[11] Fission Product Chemistry

- The tenth, and last part of this paper provides some conclusions of this work and propose the introduction of slightly improved iodine sorption model.

2 The THAI Facility

The THAI facility, acronym for ***T**hermal-hydraulic **H**ydrogen, **A**erosol and **I**odine,* is located at Eschborn, Germany. It is able to investigate stratification, convection and wall condensation as well as the heat conduction and storage in structures. Tests performed are mainly transients, governed by the thermal inertia of the large containment vessel. The facility is also characterized by a wide and complex instrumentation, allowing the determination of the thermal-hydraulics conditions inside each vessel compartment. Thanks to its characteristics THAI can be considered as an intermediate step between a separate-effect facility and a prototypical one [9] [10].

3 THAI Vessel description

The main THAI component is a cylindrical steel vessel (Fig. 1), 9.2 m high and 3.2 m in diameter, with a total free volume of about 60 m^3. The vessel could resist to pressures and temperatures up to 14 bar and 180 °C and its free volume is subdivided into six spatial zones: the sump (1.7 m^3), the bottom area (6.6 m^3), the lower and the upper annulus (11.4 m^3 and 15.4 m^3 respectively), the dome area (17.7 m^3) and the inner cylinder area (6.05 m^3) [9] [10].

The lower and upper vessel surfaces are composed by 3 cm of AISI 316 Ti, 12 cm of mineral wool and 1 mm of Aluminium, except the vessel lid which is made in St-35 steel instead of AISI 316 Ti (mineral wool and aluminium thicknesses remain the same). The estimated thermal conductivity of the insulation in the sump and in the dome areas is about 0.14 W/m·K

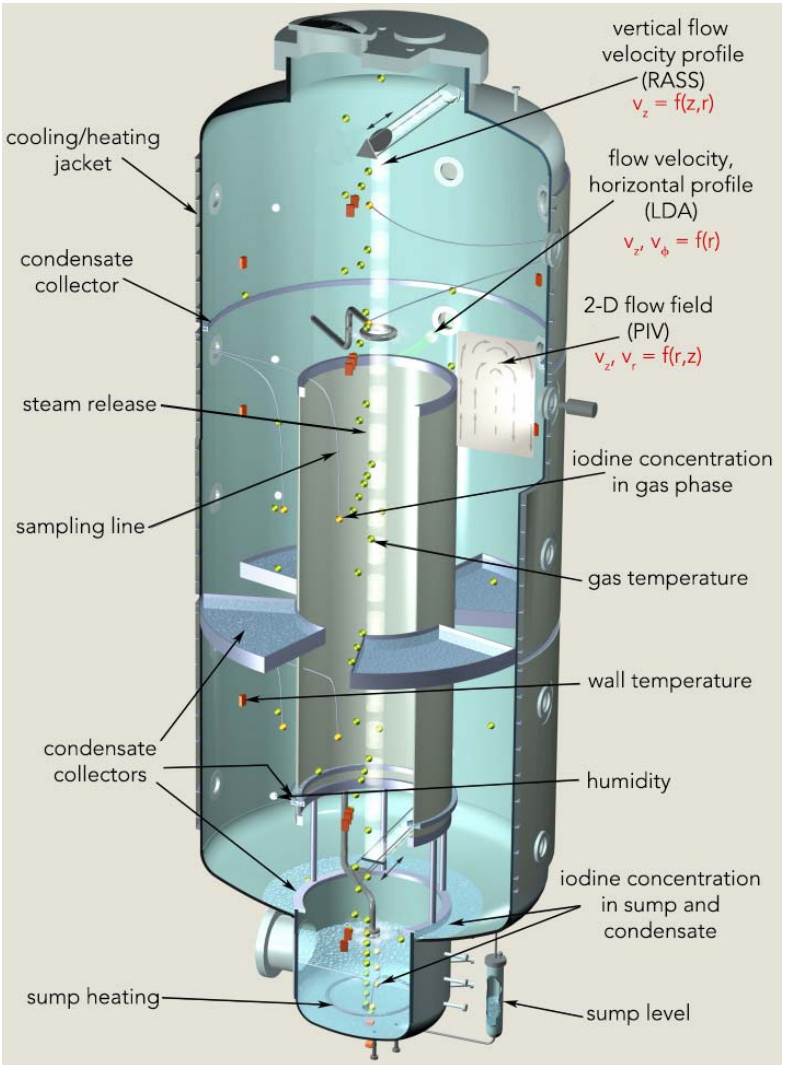

Figure 1: THAI vessel components.

The external cylindrical vessel surface is composed by three heating/cooling jackets (h/c jackets) characterized by a carrier oil moving helicoidally around the vessel circumference. Heat can also be provided to the sump water thanks to an electrical heater. The h/c jackets are composed (from the inner side to the outer side) by 2.2 cm of AISI 316 Ti, a gap of about 1.7 cm for the carrier oil, 6 mm of AISI 316 Ti, 12 cm of mineral wool and 1 mm of Aluminium. The thermal conductivity for the vertical walls insulation is 0.1 W/m·K and the thermal conductivity of the carrier oil is 1.0 W/m·K.

Moreover, during the two analysed tests, three intermediate decks of AISI 316 Ti were installed inside the vessel to enhance its spatial subdivision. The upper deck closes the inner cylinder at top and reduces the flow area from the upper annulus to the dome zone, leaving open two sections of 0.123 m^2. The intermediate deck reduces the flow area between the upper and the lower annulus,

leaving open two sections of 0.198 m^2 and 0.325 m^2. The lower deck reduces the flow area from the lower vessel zone to the inner cylinder leaving a section of 0.176 m^2. Other important vessel components are the condensate collectors, dividing the lower and the upper annulus, and the condensate gutters that drain the condensate water out of the vessel [9] [10].

4 The Iod-11 test

The Iod-11 test is characterized by eight temporal phases, covering a time span of several days. As in the SARNET benchmark specifications only 25 hours and 3 phases of the test have been simulated in the present work, i.e. from the iodine injection to the end of the mixed period (phases from 3 to 5). The other test phases are devoted to the initial preparation of the vessel atmosphere and to the final removal of the injected iodine. The main events during the Iod-11 transient are reported in the Table 1 [4] [10].

Time	Event
Phase 3 – Iodine injection	
0.0 h to 0.08 h	Injection of 0.84±0.04 g of iodine inside the dome area with air as carrier gas.
Phase 4 – Generating a mixed vessel atmosphere	
4.35 h	Middle and Lower h/c jackets switched on to heat to the vessel atmosphere.
4.7 h	Activation of the sump electrical heater.
5.32 h to 6.05 h	Helium injection (at a rate of 12 Nm^3/h) in the bottom vessel area to enhance vessel mixing.
6.4 h to 6.67 h	Middle h/c jacket gradually switched off.
6.9 h	Upper h/c jacket switched on
6.92 h	Lower h/c jacket switched off.
7.52 h	Upper h/c jacket switched off.
8.07 h to 8.45 h	Steam injection (initially a 1.4 g/s and then increased to 2.85 g/s at 8.25 h) in the bottom vessel area.
Phase 5 – Mixed vessel atmosphere	
8.58 h to 9.20 h	h/c jackets switched on (Lower at 8.58 h, Upper at 8.95 h and Middle at 9.20 h).
10.12 h	Electrical sump heater output reduced.
24.65 h	Electrical sump heater switched off and sump water partially pumped out.
24.67 h	h/c jackets switched to full cooling.

Table 1: Main Iod-11 test events.

5 The Iod-12 test

As for Iod-11, also for the Iod-12 test only 31 hours and 7 phases of the test have been simulated, i.e. from 1 h before the iodine injection to the end of the resuspension phase (from the last one hour of the phase 2 till the end of phase 7). Again, the other test phases devoted to the initial preparation of the vessel atmosphere and to the final removal of the injected iodine are not simulated. The main events during the Iod-12 transient are reported in the Table 2. It should also be highlighted that, for simplicity, in the graphs the time start at 0.0 h, which is the "-1.0 h" reported in Table 2 [4].

Time	Event

Phase 2 – Setting of test conditions	
-1.0 h	Start of the simulation
-0.32 h to -0.23 h	Injection of 0.335 Nm^3 of helium
Phase 3 – Iodine injection	
0.0 h to 0.1 h	First iodine injection in the dome area (h =8.4 m) with air as carrier gas
0.17 h to 0.21 h	Second iodine injection (same location and carrier gas)
1.75 h	Upper and middle h/c jackets switched off.
Phase 4 – Establishing a mixed vessel atmosphere	
2.62 h to 9.63 h	Injection of saturated steam (109 °C) in the upper zone of the inner cylinder area at a rate of 30 g/s, and then following increased to 34 g/s (4.0 h) and decreased to 4.3 g/s (4.82 h – 5.75 h). Furthermore the steam injection is re-increased to 6 g/s (6.95 h) and ended at 9.63 h.
2.68 h	Middle and lower h/c jackets switched on full cooling.
3.7 h	Activation of the sump electrical heater. Initially at 13.4 kW and then reduced to 3 kW (5.7 h).
4.92 h to 5.22 h	Injection of 563 g of Helium in the bottom area.
5.48 h	Upper h/c jacket switched on.
Phase 5 – Mixed vessel atmosphere	
9.67 h	Deactivation of the sump electrical heater.
9.68 h	H/c jackets thermal oil circuit switched off, but a limited cooling effect is presents due to the thermal oil natural circulation.
Phase 6 – Rest period	
-	-
Phase 7 – Iodine resuspension	
24.4 h to 30 h	Upper h/c jacket switched on full heating initially at 39 kW and then reduced to 3 kW at 25.68 h.

Table 2: Main Iod-12 test events.

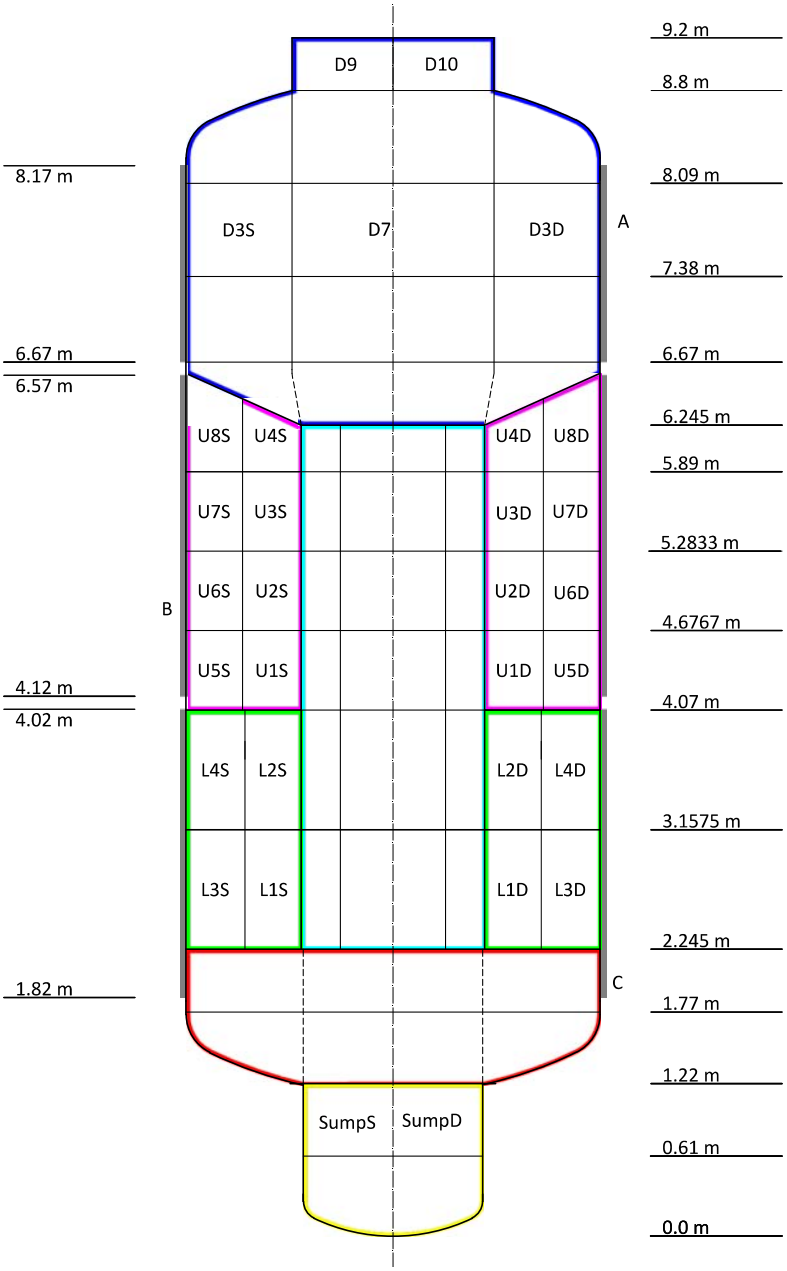

Figure 2: Nodalisation scheme.

The THAI facility has been modelled (Fig. 2) employing 66 control volumes, 60 for the vessel (3 volumes for the sump zone, 6 for the bottom area, 8 for the lower annulus, 16 volumes for the upper annulus, 14 for the dome area and 13 for the inner cylinder zone), 5 for the drain discharge volumes and 1 simulating the outer environment. The dome zone is vertically subdivided into 5 layers, while the upper and the lower annulus into 4 and 2 vertical layers respectively, with a corresponding 6 layers subdivision for the inner cylinder as in good practice guidelines for the use of lumped parameter codes [11].

These control volumes are connected with 136 atmospheric junctions, necessary for the simulation of the mass and energy exchanges among the various vessel zones. These junctions were simulated as pipes connecting the centre of the various control volumes, as stated in the user's guidelines of both codes [11] [12]. The forward and reverse loss of flow coefficients have been imposed equal to 1.0, except for the junctions connecting the lower and the upper annulus, the upper annulus and the dome area, and the bottom area and the inner cylinder, where they have been imposed equal to 3.0. Moreover, in ASTEC only, 41 drain junctions were also employed to simulate the condensate water drain, connecting the upper and lower annulus and the outer volumes of dome, the inner cylinder and the bottom area to their respective discharge volumes. On the contrary, MELCOR does not implement a drain junction model; therefore the film-tracking model was employed to simulate the condensate water route towards the external volumes.

The vessel walls have been modelled with 136 heat structures, 76 simulating the h/c jackets (24 the lower, 30 the middle and 22 the upper one). The oil has been simulated as a "solid slab" instead of a "flowing fluid", as requested in the SARNET benchmark specifications. The outer vessel temperature was imposed to 20°C, and in ASTEC also the heat transfer coefficient was set to 2' W/m^{2}K.

This quite detailed spatial nodalisation has been developed to allow the investigation of the natural circulation phenomena among the main vessel zones. Moreover, the complex nodalisation of the heat structures provide a good control of the thermal gradient among the vessel height, but at the same time makes it difficult to perform a satisfactory initial steady-state. Several sensitivity analyses has been carried out to improve this improper behaviour but not key improvements were reached, hence the initial steady-state run was not performed for both tests.

7 Iodine-steel interaction

7.1 State-of-the-art

As stated in the introduction, the state-of-the-art in the iodine steel interaction is characterized by a two-step process: a fast and reversible *physisorption* followed by a slow and irreversible *chemisorption*. The two chemical reactions explaining these two steps are:

$$I_2(g) \underset{k(2)}{\overset{k(1)}{\rightleftharpoons}} I_2(dep,s,g) \rightarrow physisorption$$

$$I_2(dep,s,g) \underset{k(4)}{\overset{k(3)}{\rightleftharpoons}} I_{FeI2}(dep,s,g) \rightarrow chemisorption$$

where:

- I_2(g) is the molecular iodine in gaseous phase (mol/l);
- I_2(dep,s,g) it the physisorbed I_2 at stainless steel surface (mol/m^2); and
- I_{FeI2}(dep,s,g) is the chemisorbed iodine at stainless steel surface (mol/m^2).

The reaction velocity can be easily calculate with the following Arrhenius equation:

$$k(i) = k_0 exp(E \frac{T - 298.15}{T \cdot R \cdot 298.15})$$

Equation 1: Arrhenius equation for the calculation of the reaction velocity values.

Where:

- k_0 is a pre-exponential constant for small temperature variations [m/s];
- E is the activation energy [J/mol];
- T is the temperature [K]; and
- R is the gas constant (8.3144 J/(mol·K).

The values k, k_0 and E necessary to calculate the four reaction velocities are reported in Table 3.

k	k_0 [m/s]	E [J/mol]
k(1)	1.8E-4	0
k(2)	1.04E-5	5.4E+4
k(3)	1.3E-4	0
k(4)	2.1E-6	0

Table 3: k, k_0 and E values needed to calculate the reaction velocity values.

However, for the k(3) value also the relative humidity effect should be included. For this purpose, the k(3) values obtained with the Arrhenius equation are multiplied with the following equation:

$$F = 0.1206 \cdot exp(0.0328 \cdot rh)$$

Equation 2: Relative humidity relation for the k(3) reaction velocity value.

Where rh is the normalized value of the relative humidity (100 % = 1.0). Subdividing the test into various sub-phases, and considering the mean vessel conditions, the k(i) values have been calculated. These values were then employed to calculate the required data needed in ASTEC and MELCOR.

7.2 ASTEC modelling (IODE)

The IODE model calculates the iodine and ruthenium behaviour in containment. The modellisation of these two radionuclides passes through the activation of the reactions involved in the performed calculation. Actually, up to 40 reactions involving both I and Ru can be activated by the user, and the adsorption of molecular iodine onto surfaces is one of them. This reaction is called "I2_sorption_steel_dry_mtr" [13] and simulates the adsorption and desorption processes as a two steps reaction. The flow of molecular iodine adsorbed onto surfaces is given in Eq. 3:

$$\Phi = k_{ads} \cdot S \cdot C_{I2}$$

Equation 3: Flow of molecular iodine adsorbed onto surfaces.

Where:

- k_{ads} is the adsorption coefficient [m/s];
- S the adsorption surface [m^2];
- C_{I2} the iodine concentration [mol/m^3].

The flow of molecular iodine desorbed from surfaces is given by the sum of thermal and radiolytic contributes, as reported in Eq. 4:

$$\Phi = -(k_{des} + DR \cdot \tau_{rad}) \cdot q_{I2}$$

Equation 4: Flow of molecular iodine desorbed from surfaces.

Where:

- k_{des} is the thermal desorption coefficient [1/m];
- DR is the dose rate [Gy/s];
- τ_{rad} the radiolytic desorption rate of I_2 from the dry stainless steel [1/Gy]; and
- q_{I2} is the number of moles of I_2 adsorbed on the surface [mol].

The k_{ads} and k_{des} coefficient can be calculated by the code or can be given in the code input deck [13]. In the present work this last option has been followed and the values utilized were calculated basing on Eq.s 1 and 2. The results of this calculation are reported in Table 4 and 5 for both the Iod-11 and Iod-12 tests.

Time [s]	ASTEC		MELCOR	
	Adsor. coeff. [m/s]	Desor. coeff. [1/s]	Adsor. coeff. [m/s]	Desor. coeff. [1/s]
0.0	4.0E-5	8.0E-7	4.0E-05	8.0E-07
90000.0	4.0E-5	8.0E-7	4.0E-05	8.0E-07

Table 4: Reaction constants for the Iod-11 test.

Time [s]	ASTEC		MELCOR	
	Adsor. coeff. [m/s]	Desor. coeff. [1/s]	Adsor. coeff. [m/s]	Desor. coeff. [m/s]
0.0	3.0E-5	3.80E-5	3.4E-05	1.0E-05
13320.0	3.0E-5	3.80E-5	3.4E-05	1.0E-05
13320.1	3.50E-5	5.10E-6	3.4E-05	1.0E-05
23400.0	3.50E-5	5.10E-6	3.4E-05	1.0E-05
23400.1	3.70E-5	5.20E-7	3.4E-05	1.0E-05
111600.0	3.70E-5	5.20E-5	3.4E-05	1.0E-05

Table 5: Reaction constants for the Iod-12 test.

Considering that IODE module just provided good results in the past SARNET investigations [4] and that the modifications implemented in the last versions [14] [15] are minor respect to the version available during the SARNET benchmark, good results are again expected.

7.3 MELCOR modelling (IP and FPC models)

Inside MELCOR three models can be employed to simulate the iodine chemistry:

- The chemisorption model. This model allows only the simulation of a single step reaction, i.e. an irreversible deposition of iodine onto surfaces. This model was not employed in this work due to its limitations.
- The IP model. This model allows the simulation of all the complex reactions involving iodine in both the gaseous and liquid phases. Thanks to its characteristic this is model has been extensively investigated in this work.
- The FPC model. This model allows the simulation of chemistry effects and can be employed to simulate fast chemical reactions, as well as two-step processes as the molecular iodine adsorption and desorption from surfaces. This model was employed in this work only for Iod-12 because the extended condensation phenomena reported in the test transport the I_2 gaseous inventory from the "aerosol" form to the "vapour" form, which cannot be simulated with the IP model.

Inside the IP model the iodine deposition and resuspension phenomena are modelled according to the Eq. 5:

$$\frac{d[I_{2wall}]}{dt} = k_{ad}[I_{2atm}] - k_{de}[I_{2wall}]$$

Equation 5: Iodine-steel reaction as modelled in the IP model.

Where:

- I_{2wall} is the wall surface iodine concentration [kmol/m^3];
- k_{ad} the adsorption coefficient [m/s]; and
- k_{de} the desorption coefficient [1/s].

The k_{ad} and k_{de} coefficients are constants for the entire transient and they can be modified through a sensitivity coefficient. If the dry wall surfaces subsequently become wet, the water film is assumed to completely dissolve the adsorbed iodine and the film can drain to other surfaces or the pool via the MELCOR film model [16]. Due to the k_{ad} and k_{de} constant nature, mean reaction velocity values calculated from the ASTEC ones have been implemented in MELCOR (Tables 4 and 5).

On the contrary, inside the FPC model, the chemical reaction can be introduced according to their stoichiometry and reaction velocities. The reaction process is modelled in MELCOR as a first-order reversible reaction for an element going from the gas phase to a surface.

$$\frac{dM_c}{dt} = -\left(\frac{\frac{(k_m \cdot A)}{V}}{\frac{(k_m \cdot A)}{(V + k_f)}}\right) \cdot \left(k_f M_g - k_r M_s\right)$$

Equation 6: Iodine-steel interaction as modelled in the FPC model.

Where:

- k_m is the mass transfer rate constant for the process, based on the mass transfer coefficient calculated by the HS Package [m/s];
- k_f is the forward reaction rate [1/s];
- k_r is the reverse reaction rate [1/s];
- A/V is the surface to volume ratio [1/m];

- M_g the iodine mass in the gaseous phase [g]; and
- M_s the iodine mass deposited onto the surface [g].

Contrary to the IP model in the FPC model both k_f and k_r values can be implemented as time vs reaction velocity tables. For this purpose, the physisorption reaction has been implemented introducing the same reaction velocities already employed in ASTEC (Tables 4 and 5) [16].

8 Iod-11 test results

In the following pages the results of the THAI Iod-11 test will be reported and discussed. For MELCOR a single case characterized by a time step of 0.5 s is here reported. This time step is slightly higher but still suitable for the analysis of the Iod- 11 transient. In detail, several sensitivity analyses were carried out to investigate the optimal time step to employ during the calculations and 0.5 s was found to be the best compromise among fast-running simulations and reliability of the results obtained.

As for MELCOR, also for ASTEC only one case characterized by a macro time-step of 1.0 s is here reported. The macro time-step is the maximum time interval in which all the modules employed in the calculation are computed at least one time. As for MELCOR several sensitivity analyses were executed and 1.0 s was found to be the optimal compromise among fast-running simulations and reliability of the results obtained.

8.1 Total Pressure & Atmospheric temperatures

During Iod-11 test the total pressure has been measured at 7.7 m in the dome compartment. The results shown by both codes are in good agreement with the experimental data, but some discrepancies can be highlighted (Fig. 2). These discrepancies can be explained considering the employed boundary conditions:

- Outer vessel surface temperature set to 20.0 °C for the entire test;
- Inner vessel surface temperatures computed by the code basing on the local thermal-hydraulic conditions.
- Power injected through the h/c jackets and the sump heater introduced with four time-vs-power tables.

In particular this last condition (power tables) could be the cause of mismatched behaviours during the mixed phase. As stated in the benchmark specifications the power injected was measured basing on the inlet and outlet oil temperatures, hence for low power injections this difference could be so small that the measurement uncertainties could not be negligible.

As it can be seen, the MELCOR results are partially different from the experimental ones (Fig. 3). These differences can be explained considering the temperature trends shown in Figure 4 to 7. At the beginning of the test in the dome area a temperature jump (Fig. 4) caused by an incorrect heat transfer coefficient calculation is reported. This behaviour is than followed by a continuous temperature decrease slightly faster than the experimental one. For this purpose, the temperature decrease trend is lost during the mixing and the mixed phases, leading also to an improper pressure trend prediction (Fig. 2).

Moreover, as reported in the Fig.s from 5 to 7, also the temperature prediction in the lower vessel zones is affected by several uncertainties. The temperature trend shown by the inner cylinder (Figure 5) is partially wrong; indeed temperature deviations from the experimental one are shown. At the end of the stratified phase a slight temperature increase is reported. Two causes can explain this behaviour: an ingress of hot fluid streams from the bottom area, or an improper heat exchange among the cylinder

itself and the upper outer annulus. However, as shown in Figure 7, the bottom area temperature is correctly predicted, and is 10 °C lower than the inner cylinder one, hence only the incorrect heat exchanges can be considered responsible for this behaviour.

On the contrary, the sudden temperature increase shown by the inner cylinder (Fig. 5) is probably due to hot streams entering from the bottom vessel zones. This behaviour is probably due to the incorrect heat exchanges toward the outer environment reported in the bottom area. In the early instant of the mixing phase two events happen in the bottom area: a helium injection occurs and the lower h/c jacket is switched on. As shown in Fig.s from 10 to 13 the helium redistribution is correctly predicted, hence only the excessive heat provided by the lower h/c jacket can be considered responsible. This hypothesis is also demonstrated by the slight temperature overestimation shown by the lower annulus (Fig. 6), which is heated by the same h/c jacket (see Fig. 2). Therefore, the prolonged temperature stratification shown by the inner cylinder, accompanied with the stronger temperature increase in the lower vessel area produced a sudden ingress of hot streams inside the inner cylinder.

After this ingress, the atmospheric conditions of the inner cylinder are completely wrong and hence the mixed phase cannot be well reproduced. Indeed, as shown in Fig. 5, the temperature trend is correctly predicted, but the values are lower than the experimental ones. At the same time also the bottom vessel area is characterized by incorrect temperature conditions, which lead to a poor prediction also in the rest phase. Moreover, at the end of the test the two zones (inner cylinder and bottom area) provides very different results. In the inner cylinder zone the temperature begins a slight increase, while the bottom area reports a slight decrease, but the experimental data reports an almost constant behaviour in both zones. This last discrepancy is probably due to the poor prediction of mass flows inside the various vessel zones. However, this hypothesis cannot be proved, because no experimental data were reported regarding the flow pattern inside the vessel. It should also be noticed that the poor temperature prediction in the bottom area and in the inner cylinder is reflected in the total pressure trend. The pressure is slightly underestimated (0.15 bar) during the rest phase as well as the temperatures in the dome, the bottom area and the inner cylinder (10 °C).

On the contrary, a special mention should be made for the lower annulus temperature (Figure 6). Also if the lower and the upper vessel zones are characterized by poor predictions, the temperature trend of the intermediate vessel zones is well reproduced. This means that the several discrepancies shown by the other vessel zones are due to local effects, which propagates only in the near zones/control volumes. As a matter of fact, the bottom and the inner cylinder behaviour seems linked together but detached from the other parts of the vessel, as well as the dome zone. At the end it can be stated that the maximum pressure discrepancy is ~0.1 bar (~5.5%) and is shown in the mixed phase at ~12 h.

Regarding the ASTEC results less complicated trends are reported. An initial pressure underestimation is shown, which is probably due to the imperfect equilibrium conditions recorded in the vessel during the initial instants of the test, especially in the dome area. In the early instant of the test the atmospheric temperatures and the structures temperatures are slightly different, especially in the dome area, hence a proper initialization of the calculation is difficult to perform. This phenomenon is clearly shown in the dome temperature, which is characterized by a slight temperature jump (5 °C - Figure 4). This jump is then followed to a fast temperature decrease compared to the experimental trend. At the same time, slight temperature increases are shown in the lower vessel zone (Fig.s 6 and 7). This different behaviour is reflected in the total pressure trend in the early instants of the stratified phase, which is characterized by a faster decrease compared to the experimental one. This fast decrease becomes slower in the final instants of the stratified phase thanks to the discording temperature trends shown by the lower and upper vessel zones.

In the mixing phase a more complex scenario is proposed. The temperature of the bottom vessel zones is characterized by fast and unrealistic increase (Fig. 7). At the same time the temperature

increase in the inner cylinder is slightly delayed. This is probably due to the an incorrect mass redistribution inside the vessel, indeed with a proper flow pattern probably the temperatures in the lower and the outer vessel zone would have increased more slowly and the temperature in the inner cylinder would have increase faster. In the meantime, the temperature prediction in the dome area is acceptable.

Finally, in the mixed phase, a quite good temperature prediction is shown in the entire vessel. However, some differences can be highlighted in the bottom area and in the inner cylinder, where the calculated trends are slightly different compared to the experimental ones. These differences are of minor importance, but their presence influences the total pressure, which continues to increase (Fig. 3).

As conclusion it can be stated that the maximum pressure difference shown by the ASTEC code is 0.5 bar (2.5%) reached at ~9.0 h, while in MELCOR a discrepancy of 1.0 bar (5%) is shown at ~11.5 h. These values are acceptable, but due to the particular vessel conditions some condensation is shown (see relative humidity in Fig. 9) in the annulus zones. However, as stated in the benchmark specifications, the vessel conditions should be characterized by a high relative humidity but without wall condensation. For this purpose it can be stated that the overall vessel conditions are not quite well reproduce, but these results are comparable to those shown in the benchmark exercise [4].

Regarding the atmospheric temperatures, greater discrepancies are shown compared to the pressure trends. In MELCOR completely wrong trends are shown in the dome and in the bottom vessel zones. The dome area seems affected by a high heat transfer coefficients, while the intermediate and lower vessel zones (upper annulus and bottom area) seem characterized by flow patterns provoking complex temperature oscillations. The only good remark could be made to the lower annulus and the lower zone of the upper annulus, where very good results are predicted. On the contrary, in ASTEC slightly better results are predicted, but some discrepancies can be highlighted in the inner cylinder and in the bottom area. The maximum temperature discrepancy in MELCOR is 20.0 °C and is shown in the bottom area twice at 7.0 h and 25.0 h, while in ASTEC a similar discrepancy is shown but only at 7.0 h.

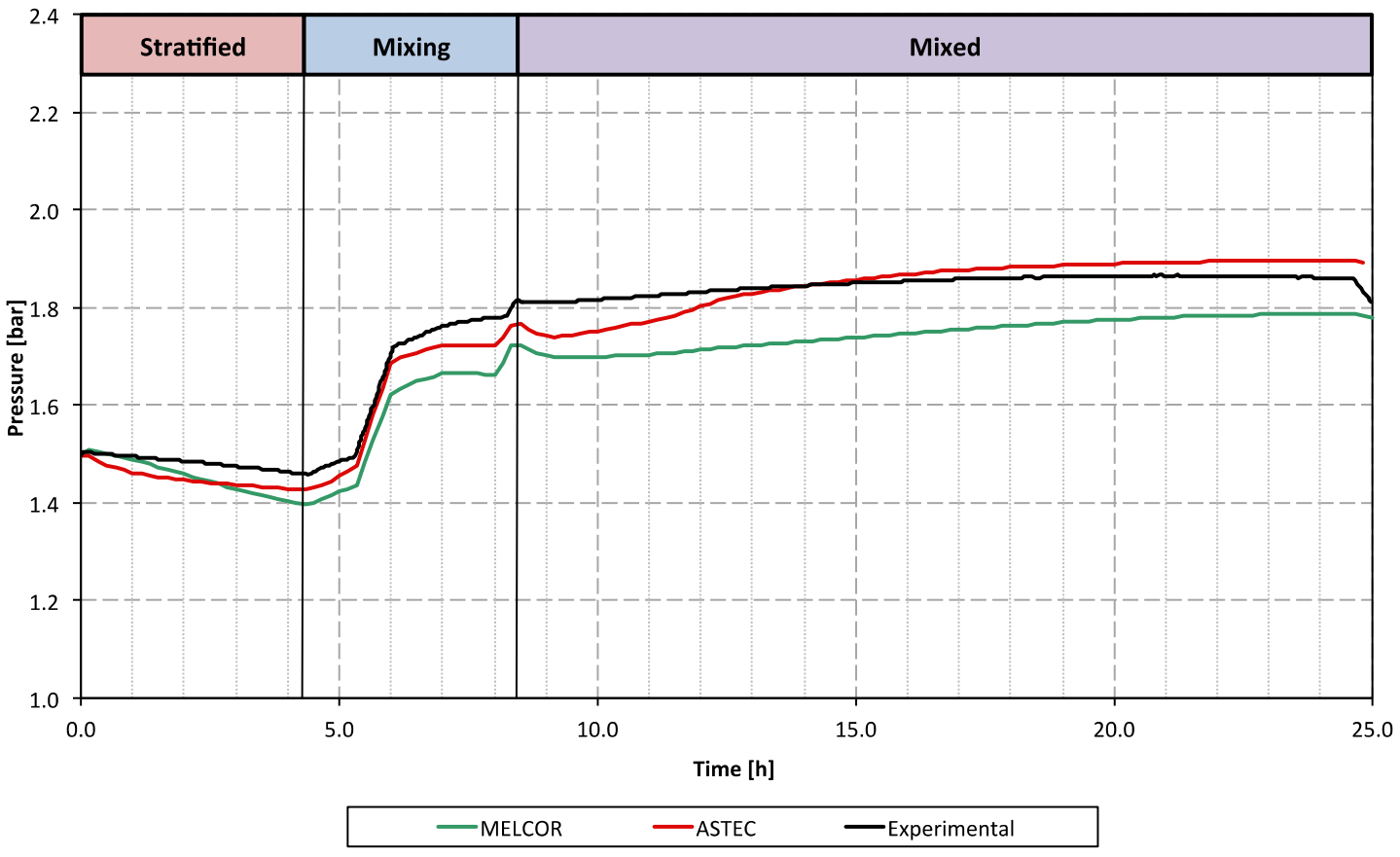

Figure 3: Total pressure in the Iod-11 test.

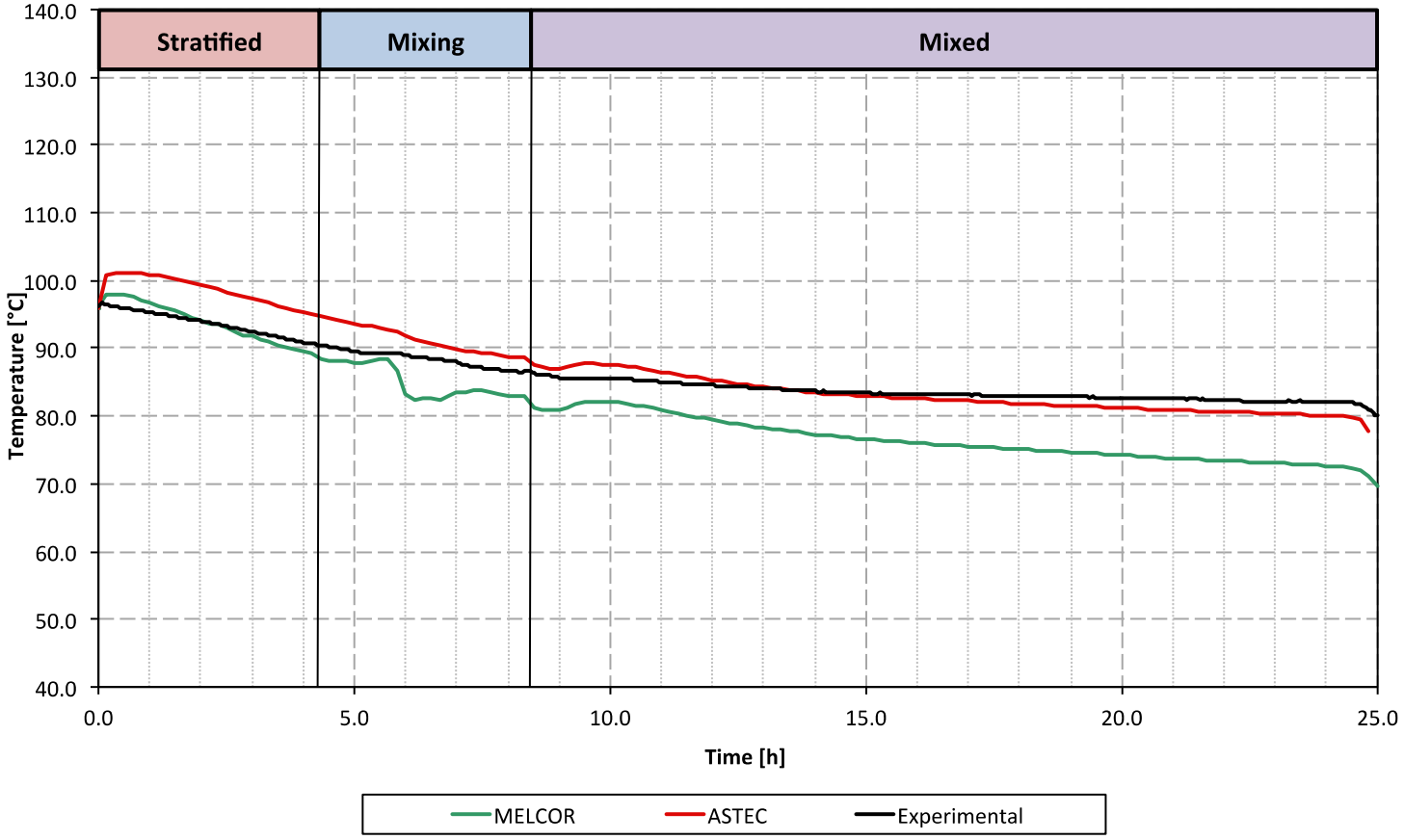

Figure 4: Atmospheric temperature in the dome compartment at 8.4 m.

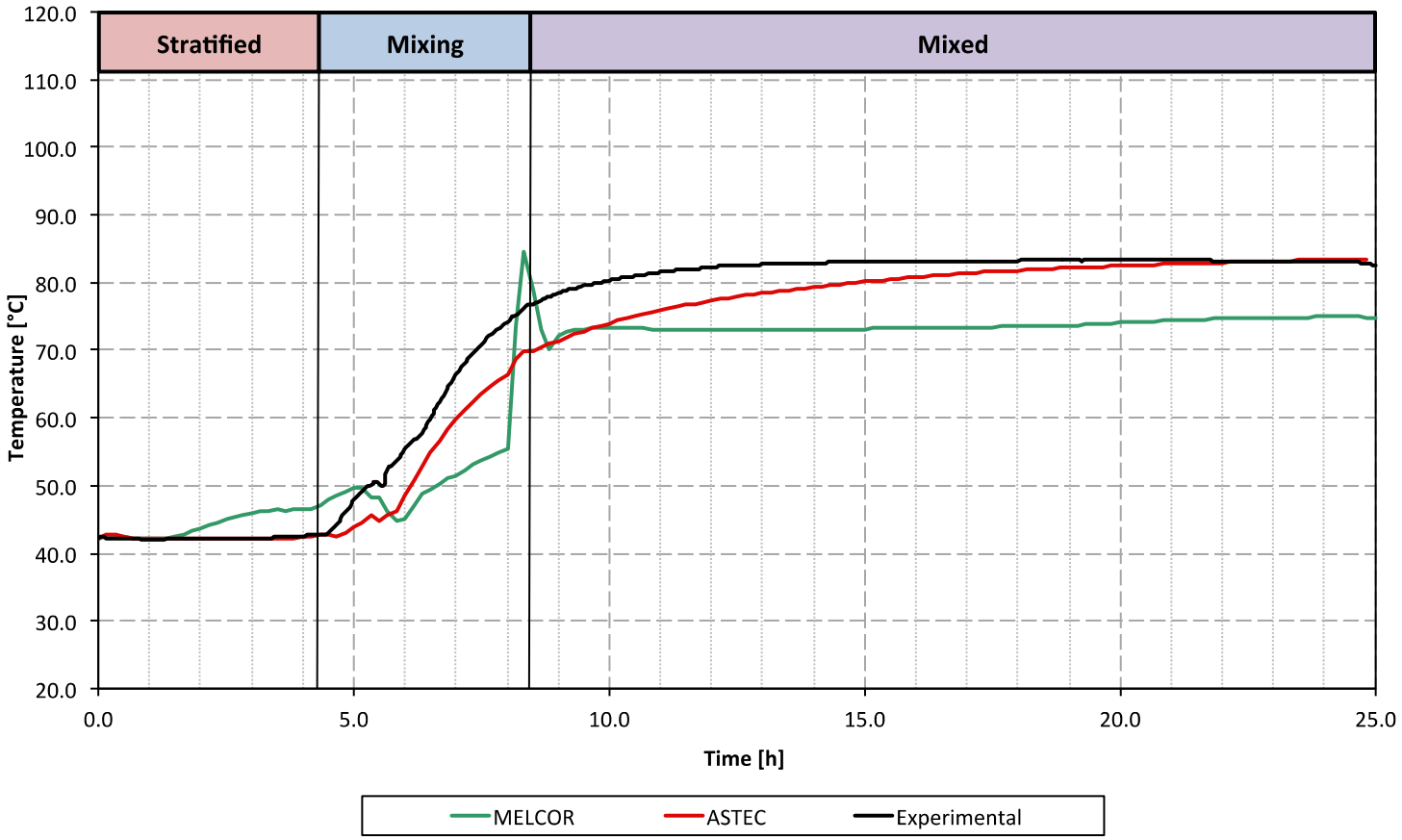

Figure 5: Atmospheric temperature in the inner cylinder compartment at 5.6 m.

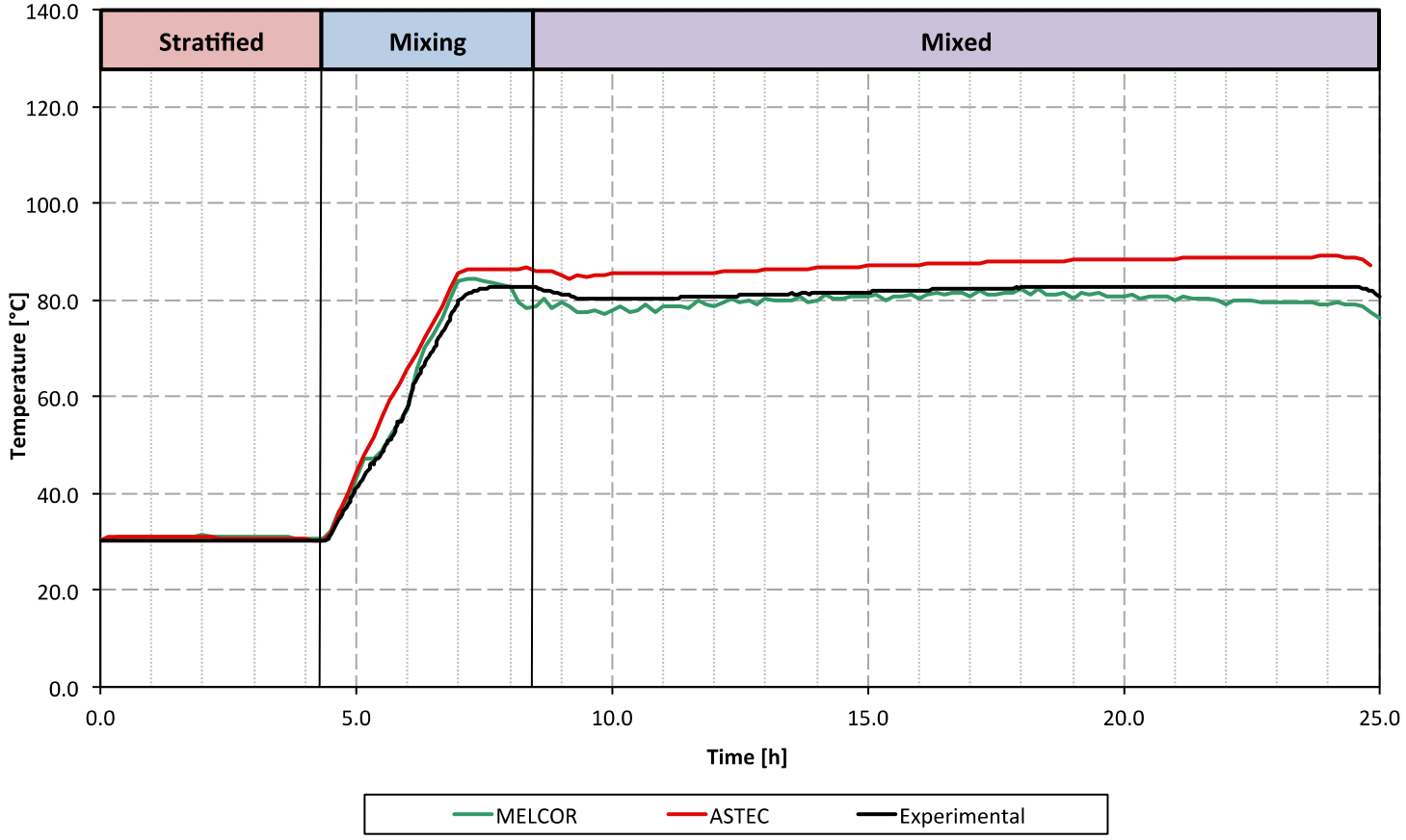

Figure 6: Atmospheric temperature in the lower annulus at 3.5 m.

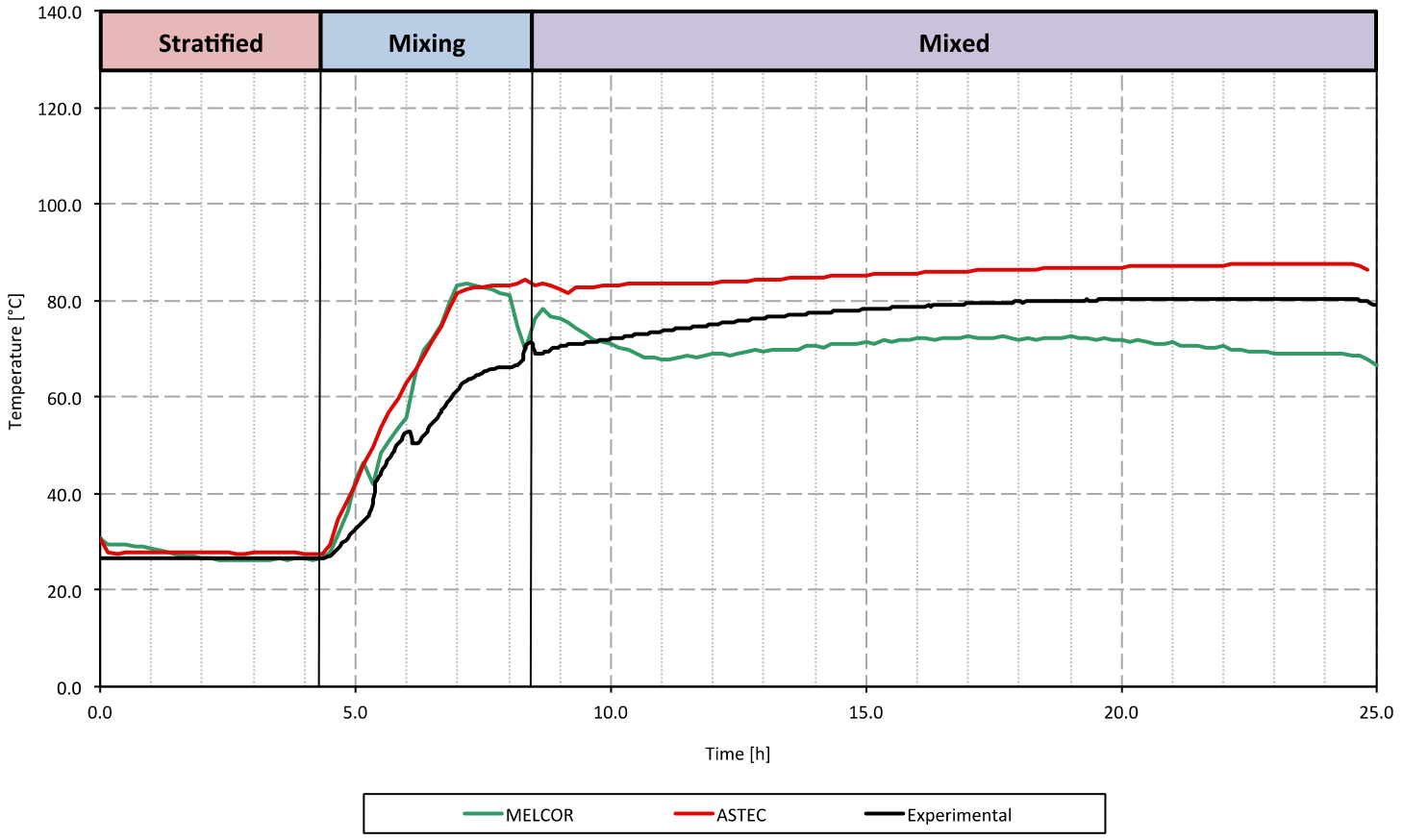

Figure 7: Atmospheric temperature in the bottom area at 2.1 m.

8.2 Relative Humidity

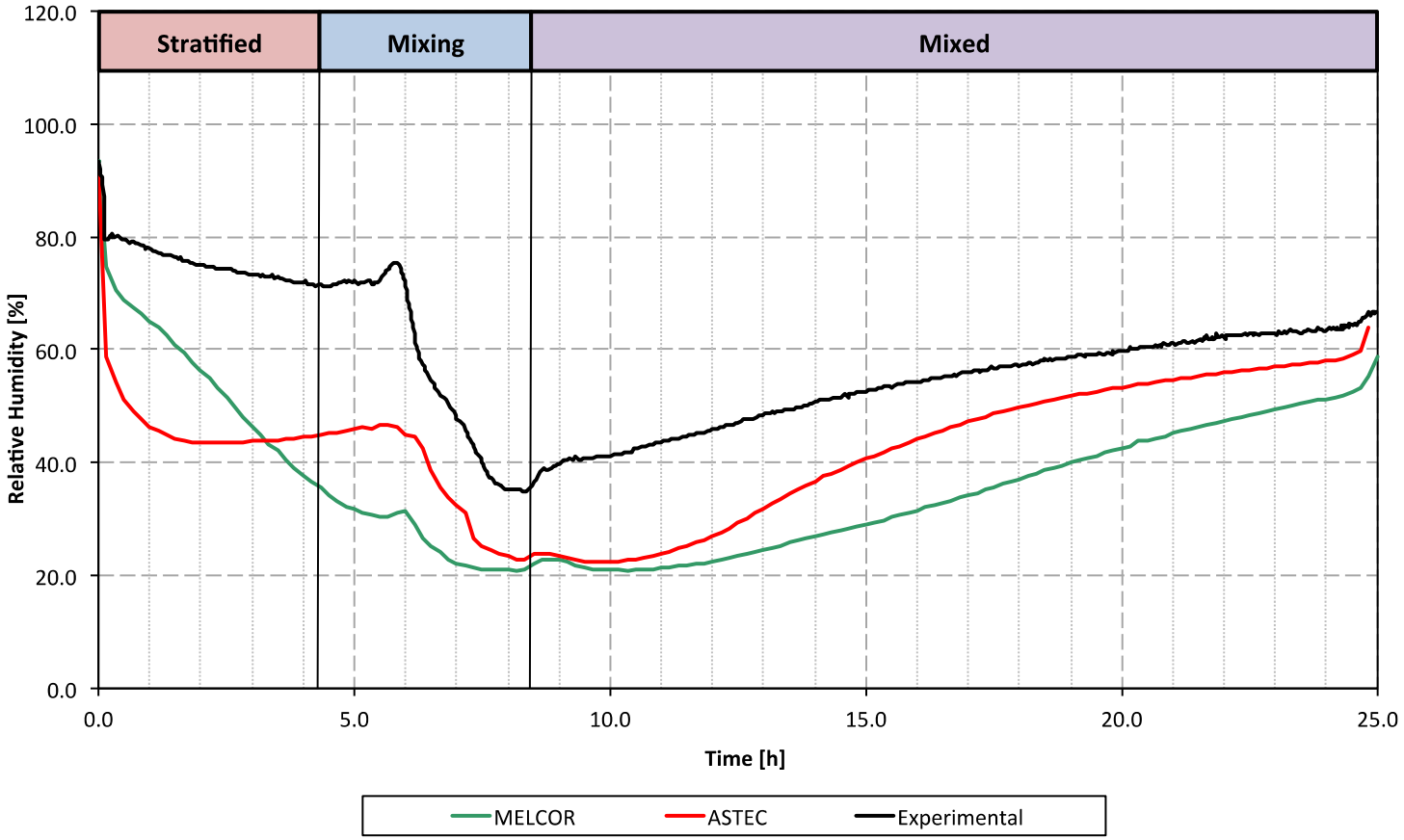

Figure 8: Relative Humidity in the dome compartment at 8.5 m.

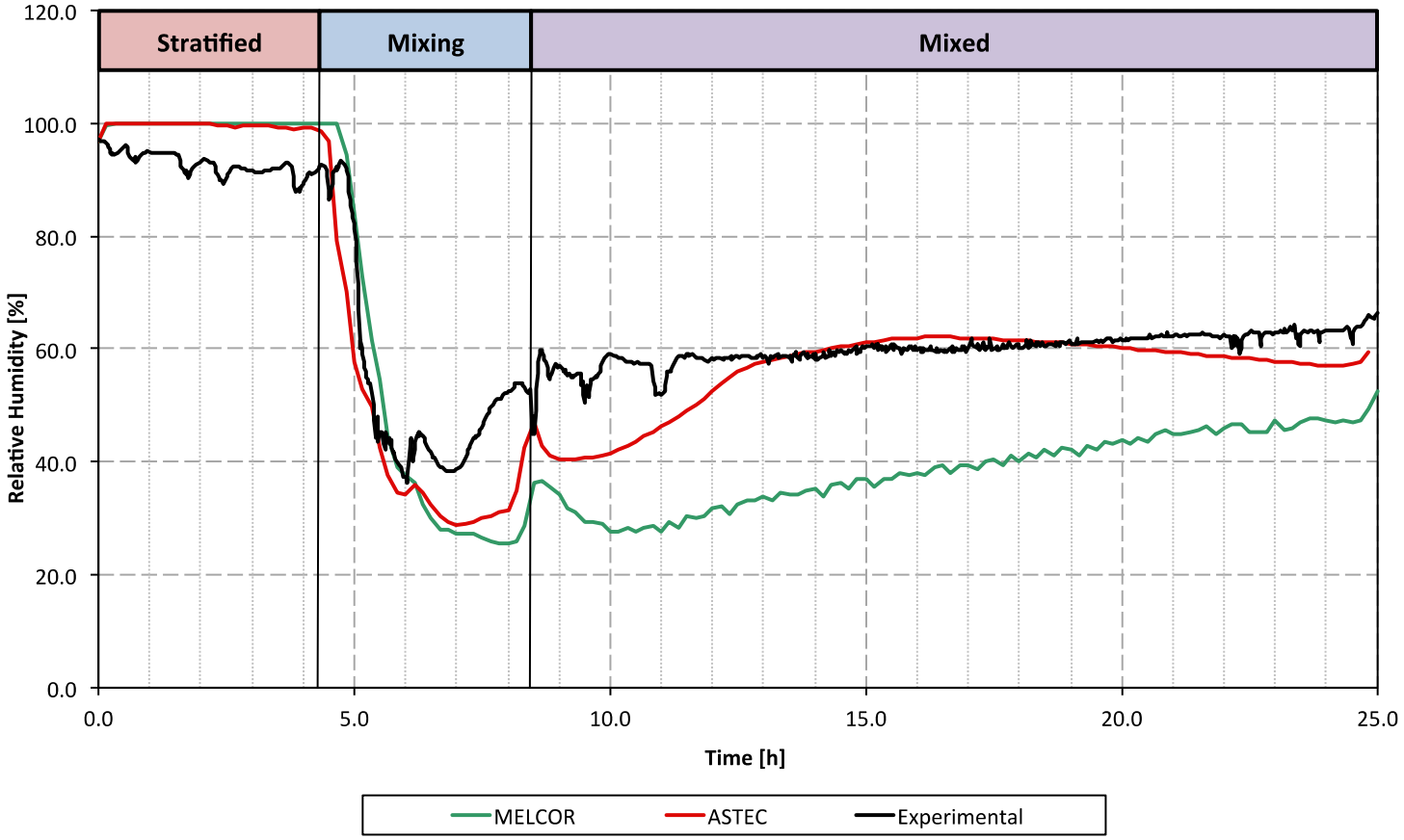

Figure 9: Relative Humidity in the lower annulus at 4.9 m.

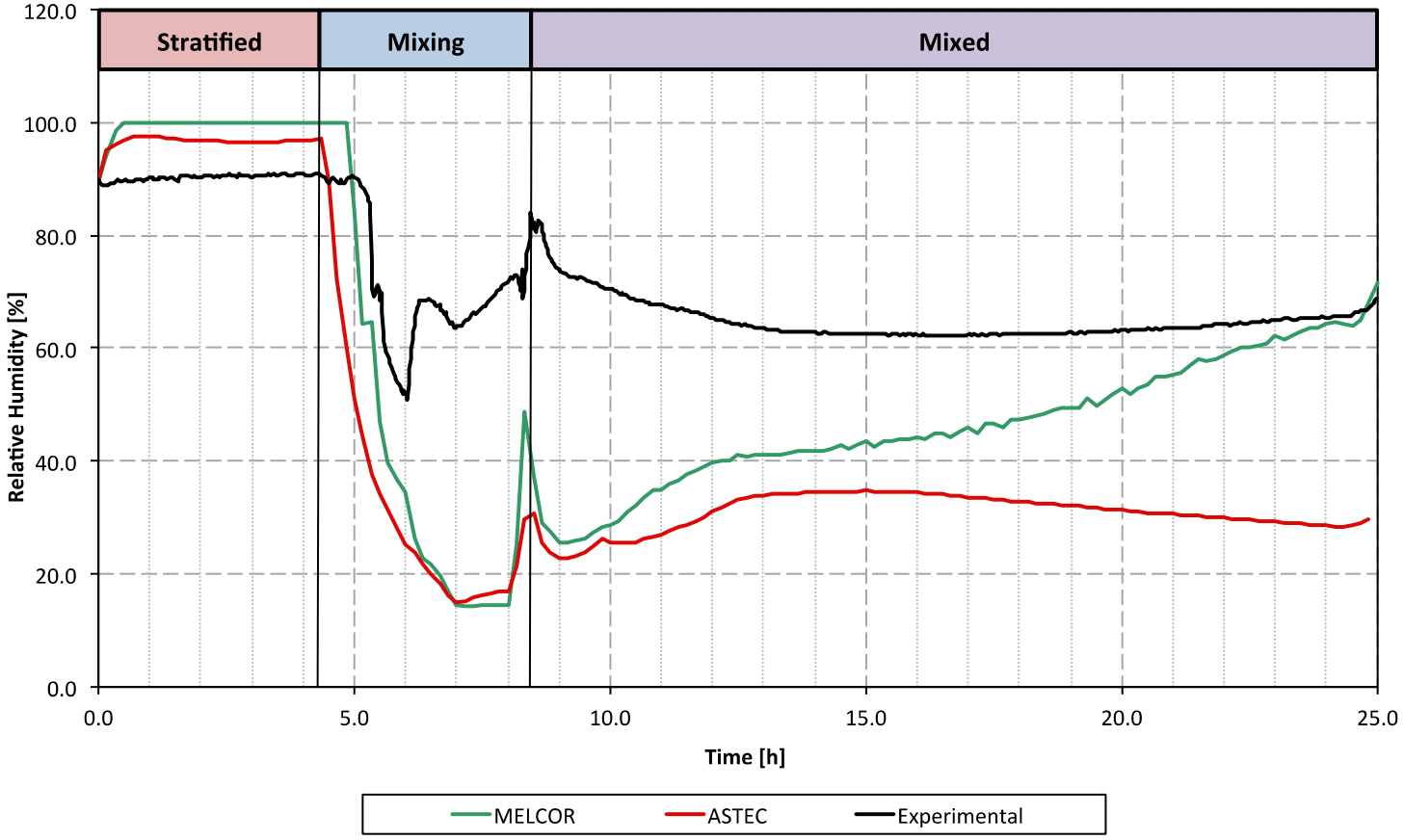

Figure 10: Relative Humidity in the bottom area at 2.1 m.

Relative humidity (r.h.[12]) is one of the most influencing parameters for the iodine-steel interaction, thus an accurate prediction for this variable is needed to correctly simulate the iodine sorption and desorption phenomena. The comparison among the experimental and the calculated data is reported in Fig.s 8 and 9 for the dome zone and the lower annulus respectively. It should be noticed that the poor predictions shown by the total pressure and the atmospheric temperatures affect the r.h. values; hence a good prediction should not be expected.

In MELCOR, as shown in Fig. 8, the dome r.h. is underestimated for the entire transient (5% – 45%). This behaviour could not be fully explained considering that in the early hours of the transient is predicted a higher atmospheric temperature compared to the experimental one. For this purpose, the r.h. trend of the upper annulus and the bottom area are reported (Fig.s 9 and 10). As it can be seen, in the upper annulus and the bottom area a continuous condensation is shown (r.h. at 100%). This behaviour is completely wrong, and could be the best explanation for the continuous r.h. decrease in the dome area. During the stratified phase the atmospheric temperatures are well predicted, hence a continuous ingress of steam should be the only cause to explain this behaviour. The continuous r.h. decrease fits well with this hypothesis, but it cannot be stated if it is the continuous steam pumping from the upper vessel zone the cause of the condensation phenomena in the lower vessel zones, or if it is the condensation the cause of the continuous steam pumping.

On the contrary, the r.h. trend at 4.9 m is well predicted in the mixing phase, while in the dome area it suffers for the initial inconsistent behaviour. Finally, in the mixed phase, the r.h. trend starts to increase faster than the experimental one. This behaviour can be explained considering that the temperature decreases faster than the experimental one and the pressure increase is not strong as reported in the experimental results, thus the combination of these two trends could lead to improper r.h. behaviours.

[12] Relative Humidity

On the contrary, the r.h. at 2.1 m is completely wrong during both the mixing and the mixed phase (errors spanning from 10% to 50%). In the mixing phase a higher decrease is shown, while the mixed phase is characterized by an incorrect trend. This is probably due to the poor temperature prediction in the bottom vessel zone, which is characterized by an unexplained decrease after 16 h.

Regarding ASTEC, some differences can be discussed. As it can be seen, in the stratified phase a similar trend compared to MELCOR is shown, although the condensation phenomena are concentred only in the annulus zones. This "steam sink" provoke a continuous r.h. fall in the upper vessel zone, but this behaviour is less pronounced compared to MELCOR. Moreover, these condensation phenomena happen only during the first two hours of the transient, hence the good trend prediction shown in two graphs strengthen the "steam sink" hypothesis.

Following, as for MELCOR, the mixing phase is somewhat well predicted. The trends shown in Fig.s 8, 9 and 10 are comparable to the experimental ones, but the values are slightly different de to the poor prediction of the stratified phase. On the contrary, the mixed phase is characterized by a very strange behaviour, which cannot be explained considering only the differences shown by the total pressure and the atmospheric temperatures. For this purpose, a joint influence of mismatched temperatures and total pressure plus complex flow pattern seems to be the most realistic explanation.

As conclusion it can be stated that the r.h. trends are not well predicted due to the poor results obtained in term of total pressure and atmospheric temperatures. Nevertheless, complex flow patterns could take part to these mismatched trends and results. However, a better prediction of the atmospheric temperature would have increased the predictions of both the pressure and the r.h. trends. Regarding the MELCOR and the ASTEC runs, the maximum error is shown at the end of the mixing phase at 2.1 m, in which an underestimation of around 40% is shown. Finally, it could be also noticed, that similar discrepancies in term of values have been also shown in the benchmark exercise [4].

Moreover, the r.h. is one of the most influencing parameter for the iodine-steel interaction; hence these poor results will negatively influence the overall iodine behaviour. However, due to the approach followed to calculate the reaction velocities (see section 7), its effect has been reduced, thus good iodine results could be expected, also if the thermal-hydraulic results are unsatisfactory.

8.3 Helium concentration

Helium has not a direct influence on the iodine-steel interaction but its presence enhances the stratification break during the mixing phase and the subsequent iodine spatial distribution. Moreover, helium can be also used as tracer material to show how and when the mass redistribution occurs during the test. In Fig.s 11, 12, 13, and 14 the helium concentrations in several locations are shown.

As reported in Fig.s 11, 12, 13, and 14, several differences can be highlighted, especially in the late instants of the mixing phase. As shown in Fig. 11, the helium concentration is slightly underestimated, while in bottom and the inner cylinder zones higher concentrations are reported. This means that the flow pattern are not well reproduced, indeed helium flows preferentially inside the inner cylinder instead of the upper vessel zones.

This incorrect initial redistribution influences also the early instants of the mixed phase, which is characterized by an unrealistic behaviour. In the dome area a helium concentration increase is shown, while in all the other zones the helium concentration decreases. This means that also at the beginning of the mixed phase an incorrect flow pattern is predicted. However, in the long term, the concentration values and trends start to be comparable with the experimental ones, except for the MELCOR run in the inner cylinder. However, it should be highlighted that the helium concentration is calculated basing on the He partial pressure; hence also the discrepancies shown in the total pressure could influence the He concentration in the various vessel zones.

As conclusion it can be stated that some differences are shown in the He concentrations. These differences are mainly due to an incorrect flow pattern inside the vessel, which directs He inside the inner cylinder instead of upper vessel zones. This leads to an overall overestimation of about 3.0 % (absolute value) in both codes, which influences the early instants of the mixed phase, but at the end of the test quite good results are shown, except for MELCOR. The He concentration is calculated basing on the partial pressure and the total pressure, hence the numerical differences can be explained considering that also the total pressure is not well reproduced in the MELCOR run. It could be also noticed that these mismatched trends reaffirm the hypothesis of the incorrect mass flow pattern already pointed out to explain the incorrect r.h. results.

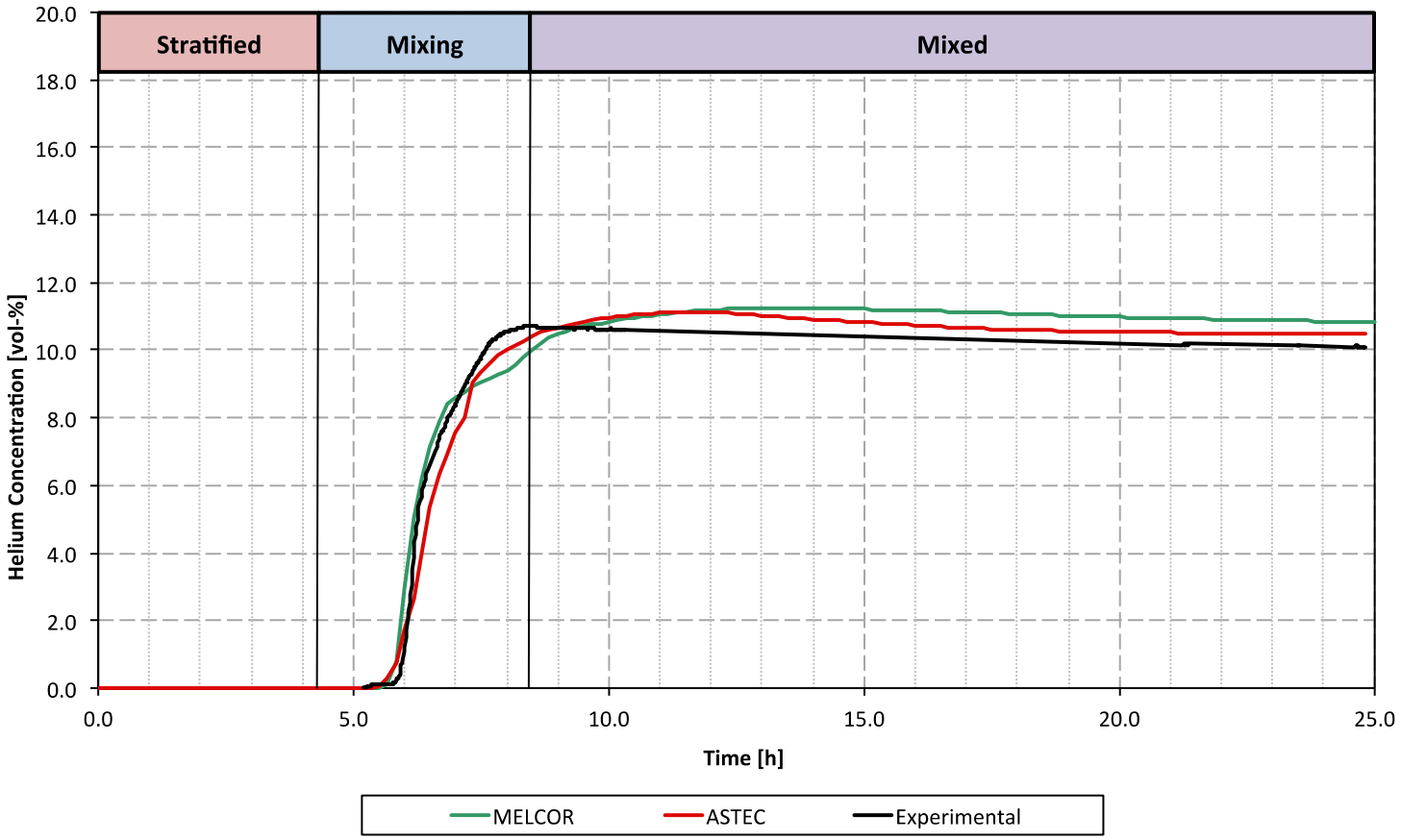

Figure 11: Helium concentration in dome area at 8.7 m.

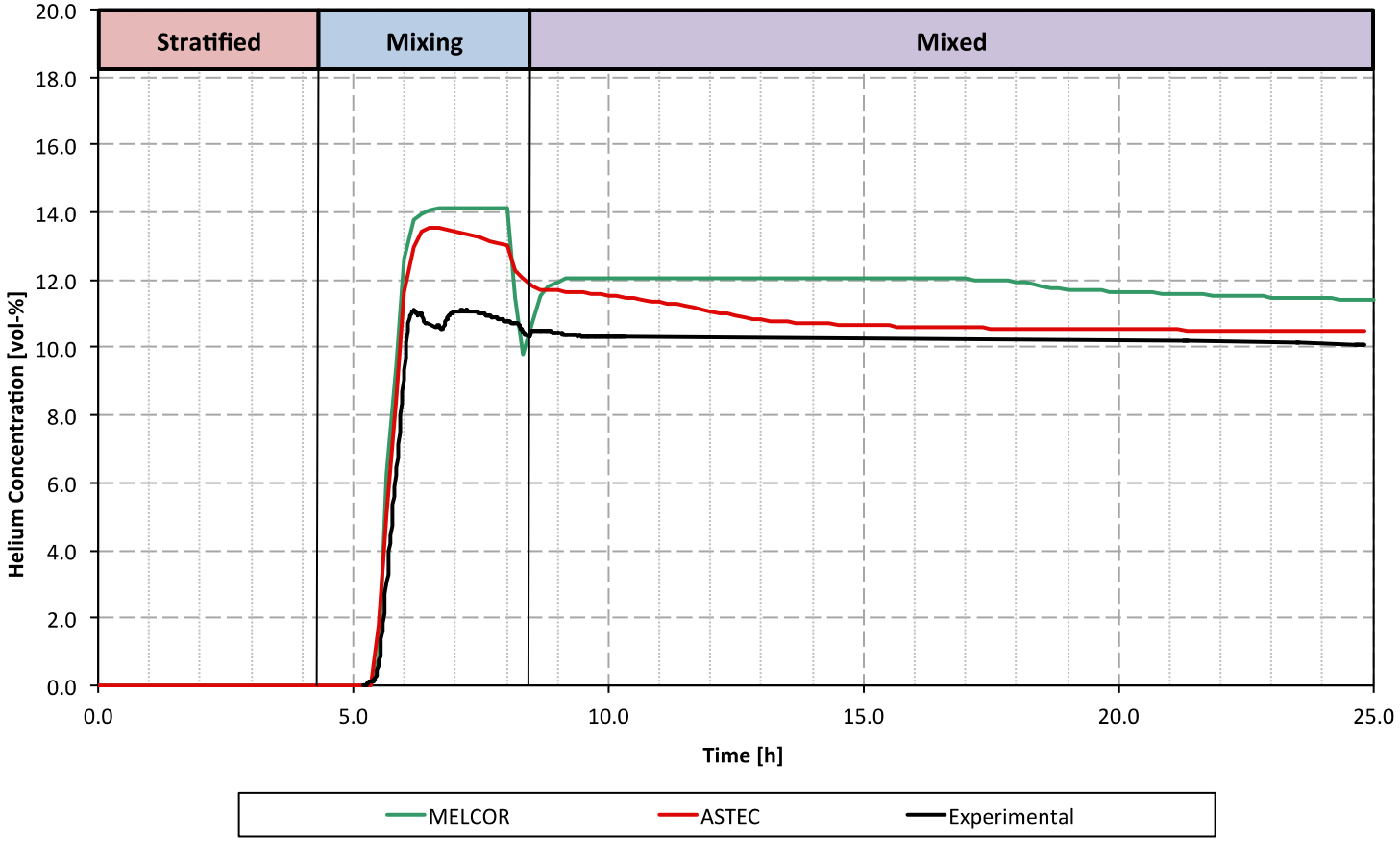

Figure 12: Helium concentration in the inner cylinder compartment at 5.4 m.

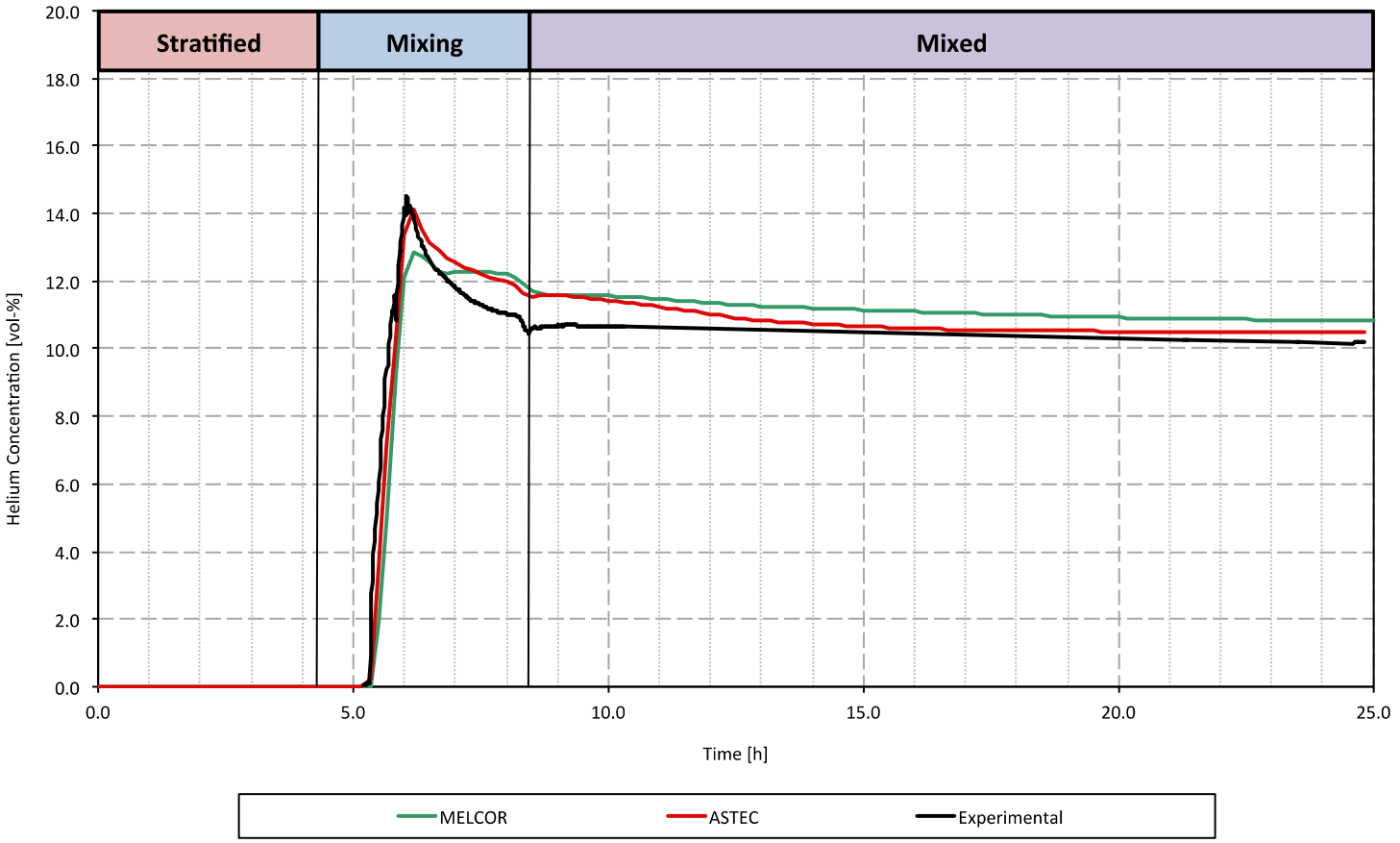

Figure 13: Helium concentration in the upper annulus at 4.6 m.

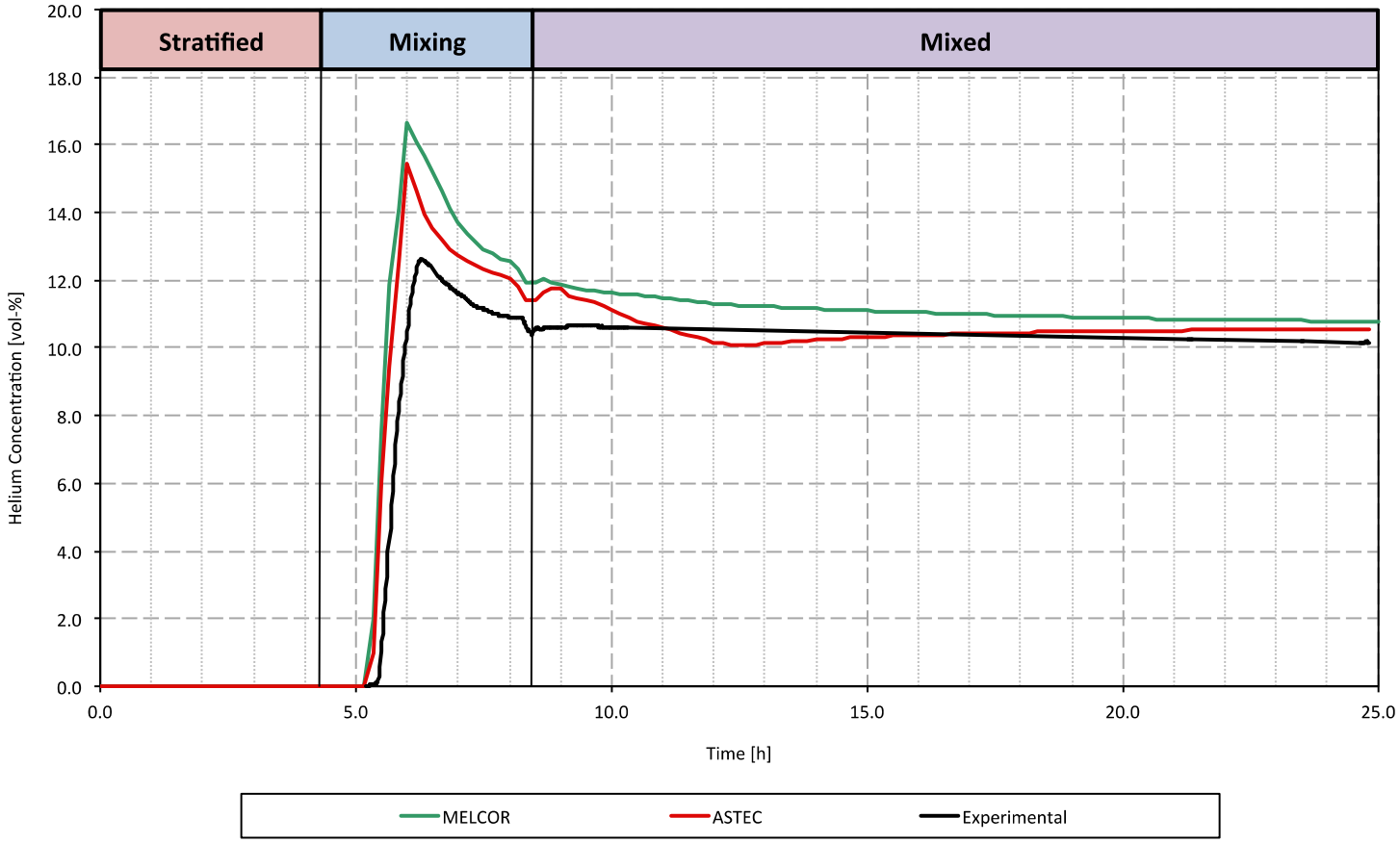

Figure 14: Helium concentration in the bottom area at 1.7 m.

8.4 Iodine gaseous concentration

The iodine gaseous concentration is the simplest experimental data permitting the check of the iodine transport and deposition phenomena within the THAI containment vessel. Therefore a good agreement between experimental and calculated data is the best indication for the correctness of the iodine-steel interaction model. The iodine gaseous concentration has been measured at various heights inside the THAI vessel during the test, however here only the data referring to three locations are reported (8.7 m, 5.3 m, and 1.8 m). As stated in the iodine-steel interaction modelling section, the reaction velocities have been calculated basing on the experimental data, hence the incorrect trends shown in term of temperatures and relative humidity do not influence the iodine-steel interaction. However, this approach can be followed only on open benchmarks as Iod-11 and Iod-12. For this purpose a new approach to introduce the parameters needed to simulate the iodine interaction is reported inside the conclusions.

As shown from Fig. 15 to Fig. 17, in the stratified phase both codes present an iodine transport toward the lower vessel zones, which is not highlighted in the experimental results. During this first 5.0 h the main event influencing the iodine concentration is the vessel atmosphere mixing. Therefore, these initial incorrect trends highlight a vessel in which the temperatures are well stratified (Fig.s from 4 to 7), but continuous mass exchanges happen. Moreover, the higher iodine concentrations shown in the lower vessel zones should be accompanied with lower iodine concentration in the dome area. However, this phenomenon is not highlighted at 8.7 m (Fig. 15), hence probably the concentration underestimation is shown only in the zones under this height (not reported here). The maximum difference shown in this phase is around three orders of magnitude (1.0E-5 g/l instead of 2.0E-8 g/l in the upper annulus) for

ASTEC and two orders of magnitude for MELCOR (1.0E-.6 g/l instead of 2.0E-8 g/l in the upper annulus).

Following, in the mixing phase both codes predict incorrect trends. In ASTEC the dome area is characterized by a faster iodine concentration decrease compared to the experimental one, while in the lower vessel zones the concentration decreases instead of increase due to the incorrect prediction during the stratified phase. Similarly in MELCOR the concentration in dome area decreases faster than expected, providing a discrepancy of one order of magnitude compared to the experimental results. A similar behaviour is also shown in the lower vessel zone, where the concentration falls below 1.0E-8, which is the minimum detectable by the iodine samplers in the vessel. This behaviour is surely due to an incorrect flow pattern, which pushes iodine inside the inner cylinder (not reported here, but demonstrable with the helium concentration trends, which are good indicators of the flow pattern inside the vessel). However, at the end of the mixing phase, quite good results are measured inside each vessel zone in ASTEC, while in MELCOR in the lower vessel zones the iodine concentration is well below the experimental results.

Finally, during the mixed phase, the results shown by ASTEC are in good agreement with the experimental ones. This phase is mainly influenced by the iodine-steel interaction, being the vessel in rest conditions. The good results shown mean that a uniform reaction velocity along the entire vessel is able to correctly simulate the iodine behaviour.

However, in MELCOR a concentration increase is measured in all the bottom area and in the annulus zones. This unexpected increase is probably due to the ingress of iodine from the inner cylinder to the bottom vessel area and following in the upper annulus. At 10.0 h the values shown by MELCOR are comparable to the experimental ones in the bottom area, while in the upper annulus and the dome an underestimation of one order of magnitude is reported. Finally, these discrepancies continue to be reported till the end of the test.

As conclusion it can be stated that in ASTEC the maximum concentration error is reported in the annulus zone at the beginning of test. The incorrect flow pattern predicted by the code is the main cause of this behaviour, and the maximum difference shown is around 3 orders of magnitude. Similarly, also MELCOR predicts these higher iodine concentrations at the beginning of the test, but the most important discrepancy is the fast concentration decrease in the mixing phase experienced in the lower vessel zones. For this purpose, it can be stated that the IP model is only partially able to predict the iodine behaviour, hence only the chemisorption model seems to be suitable to simulate iodine [4].

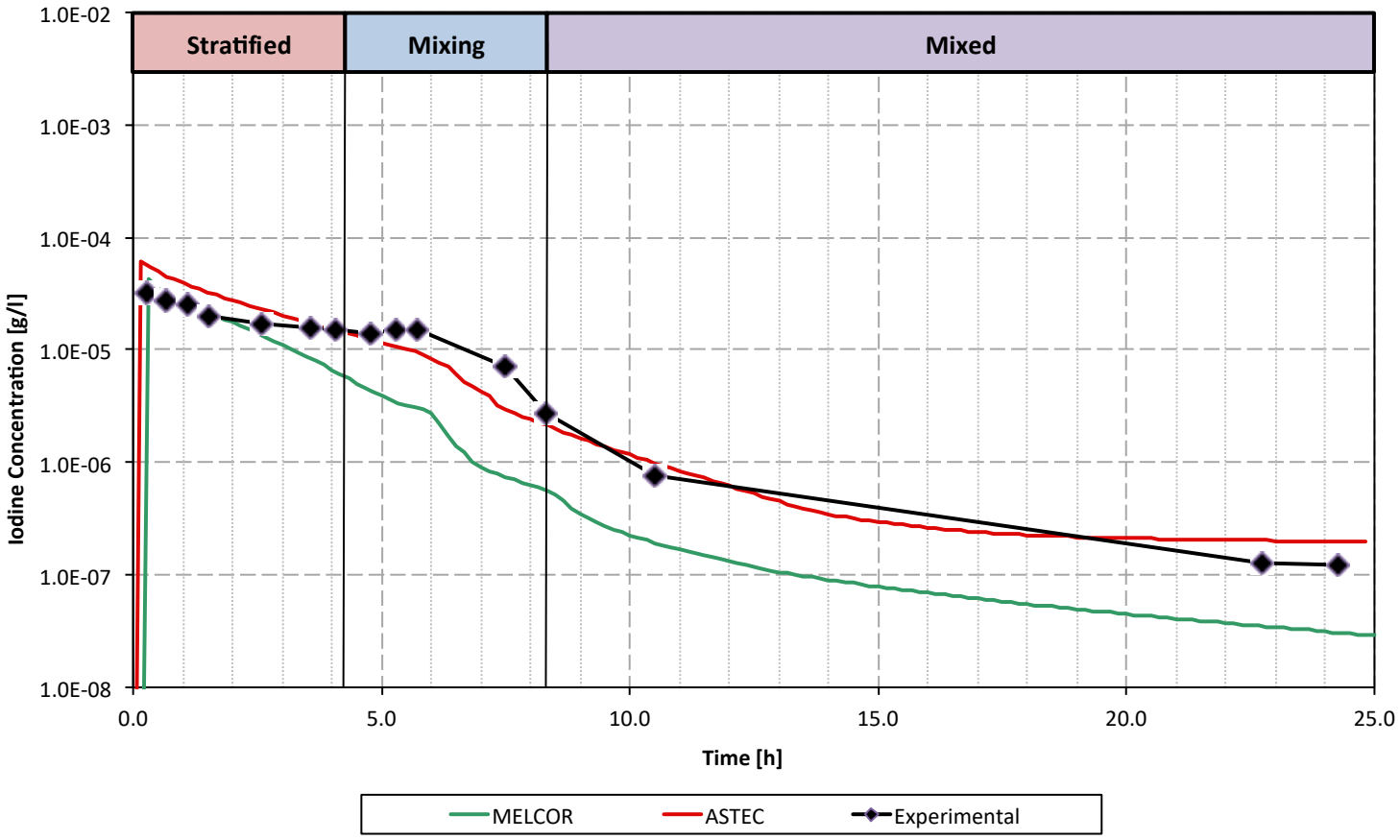

Figure 15: Iodine gaseous concentration in the dome area at 8.7 m.

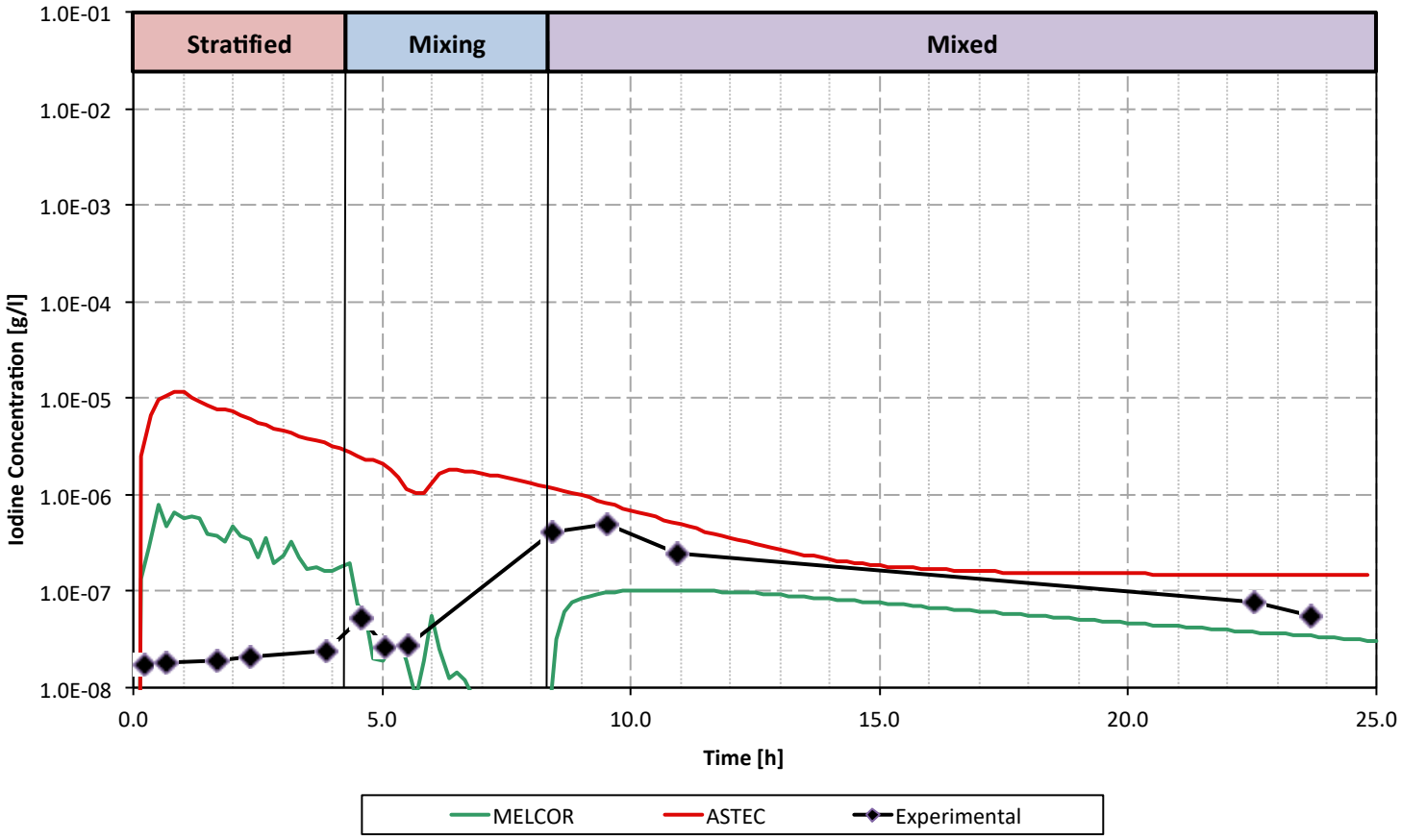

Figure 16: Iodine concentration in the upper annulus at 5.3 m.

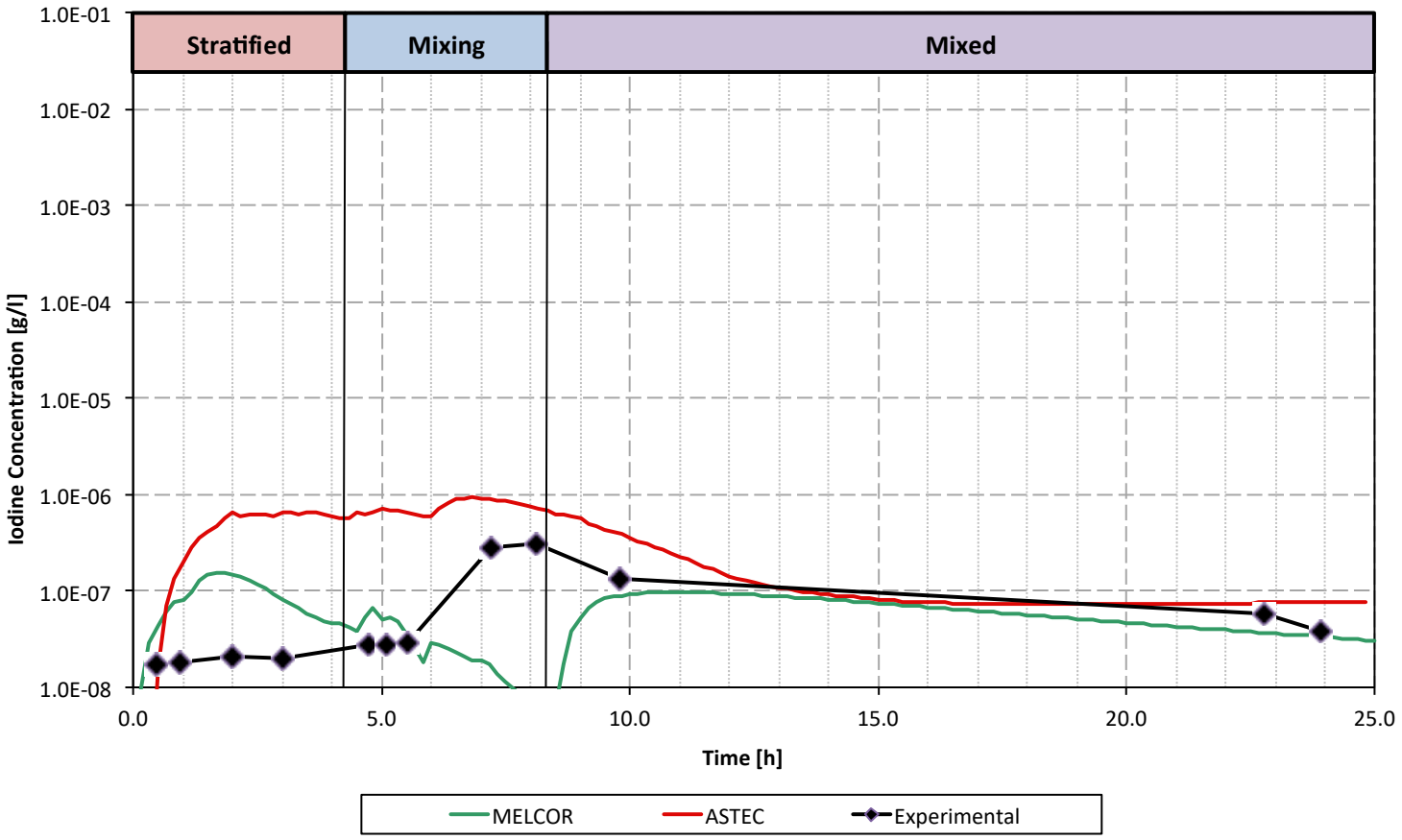

Figure 17: Iodine concentration in the bottom area at 1.8 m.

9 Iod-12 test results

In this section the results of the THAI Iod-12 test will be reported and discussed. The main difference between the two THAI tests is the presence of wall condensation phenomena providing, in Iod-12, an additional I_2 transport mechanism towards the walls and so influencing the overall iodine behaviour.

It should be also highlighted that, compared to Iod-11, more detailed analyses were carried out on the MELCOR code to solve the problems shown by the iodine models investigated. Three cases were investigated:

- The first case in which only the IP model was activated;
- The third, and last, case in which only the FPC model was activated.
- The third, and last, case in which both the IP and the FPC models were activated;

The second and the third cases were investigated because the condensation reported in several vessel zones produces the transport of iodine from the "aerosol" to the "vapour" form, which cannot be treated by the IP model. For this purpose the joint activation of the IP and the FPC models was executed, but several numerical errors were experienced. To investigate the causes of this behaviour another run characterized by the activation of the only FPC model was executed. After several sensitivity analyses no solutions were found to allow the correct simulation of the iodine behaviour, but only a minor time step effect was noticed. Therefore, in the following these three cases will be reported and discussed.

9.1 Total pressure & Atmospheric temperatures

As in Iod-11 the total pressure was again measured at an elevation of 7.7 m inside the dome area (Fig. 18). Compared to Iod-11 test, the absolute total pressure error shown is higher for both codes, but it could be noticed that the pressure spans from 1.4 bar to 2.5 bar instead of 1.45 – 1.85 bar as in Iod-11. For this purpose, higher absolute errors could not lead to higher relative errors, and thus under some aspects the Iod-12 results could be better predicted.

As it can be seen from Fig. 19 to 22, the atmosphere temperatures are well predicted in all the zones during the entire test. Only the following differences can be highlighted:

- In the bottom area during the mixing and the mixed phases. The discrepancies shown in the mixing phase are probably due to the excessive steam transported inside it (the steam injection occurs in the inner cylinder).
- In the mixing phase in the annulus zones. This behaviour is due to the same cause of the bottom area overestimation, indeed steam enters also in these zones increasing the atmospheric temperature. However, this phenomenon is less pronounced compared to the bottom area.
- In the mixing and the mixed phase the dome temperature in MELCOR is slightly underestimated, but this discrepancy tends to be negligible during the rest phase. Following, in the resuspension phase, the atmosphere temperature is overestimated in both the ASTEC (18 °C) and the MELCOR (10 °C) codes. This behaviour is shown thanks to the heat provided by the upper h/c jacket, but due to the incorrect heat transfer coefficients calculated by both codes a higher part of this heat is routed toward the vessel instead of the outer environment.
- From 15.0 h to the end of the test MELCOR predicts slightly higher temperatures, but the overall trends are good. This is due to the incorrect prediction of the temperature decrease at the end of the mixing phases (Fig.s from 20 to 21) or during the mixing phase (Fig. 22).

In both codes the mixing and the mixed phases seem the most challenging to be reproduced, and thus the maximum absolute error of the total pressure is reported here (0.2 bar in ASTEC and 0.1 bar in MELCOR). All the differences highlighted in the atmospheric temperatures influence the total pressure trend, but during the mixing and the mixed phases also the condensation rates (not reported here) are of main concern. Indeed, the discrepancies shown in term of atmospheric temperatures cannot justify the total pressure trends at all. In particular, the excessive condensation in the sump seems to be the most reasonable hypothesis to demonstrate this behaviour. In the inner cylinder zone the steam condensation seems underestimated, thus a higher part of this steam is routed to the bottom zone, which in turn routes this steam to the annulus zones and to the sump. For an incorrect flow pattern prediction the bigger part of this steam is directed to the sump zone (where it condense), instead of the annulus and the dome zones, and thus the contribute of the steam partial pressure to the total pressure is lower than expected. This phenomenon provokes an underestimation of the relative humidity in the upper vessel zones (Fig.s 23 and 24), and hence an underestimation of the vessel total pressure. This phenomenon is more pronounced in the ASTEC calculation, indeed a higher total pressure error is predicted compared to the MELCOR run (0.2 bar in ASTEC and 0.1 bar in MELCOR).

Finally, in the rest and resuspension phases the total pressure trends are slightly different from the experimental one. In the early instants of the rest phase the total pressure decreases as shown in the experimental results also if the atmospheric temperatures trends are not in good agreement with the experimental ones. Following, in the late rest phase, the pressure trends shown by both codes do not decreases as in the experimental one, and thus similar numerical values are predicted at 25.0 h (discrepancy less than 0.05 bar). The resuspension phase is then well reproduced by both codes.

As conclusion it can be stated that some differences are highlighted for both the total pressure and the atmospheric temperatures, but this differences are less pronounced compared to Iod-11. The maximum pressure difference is shown for both codes during the mixing phase and is 0.2 bar for

ASTEC and 0.1 bar for MELCOR. On the contrary, the maximum difference in term of atmospheric temperatures is shown for both codes at the end of the test and it is 18 °C for ASTEC and 10 °C for MELCOR. These differences, especially the temperature ones, could influence the overall iodine-steel interaction, but thanks to the approach employed to calculate the reaction velocities their influence should be reduced.

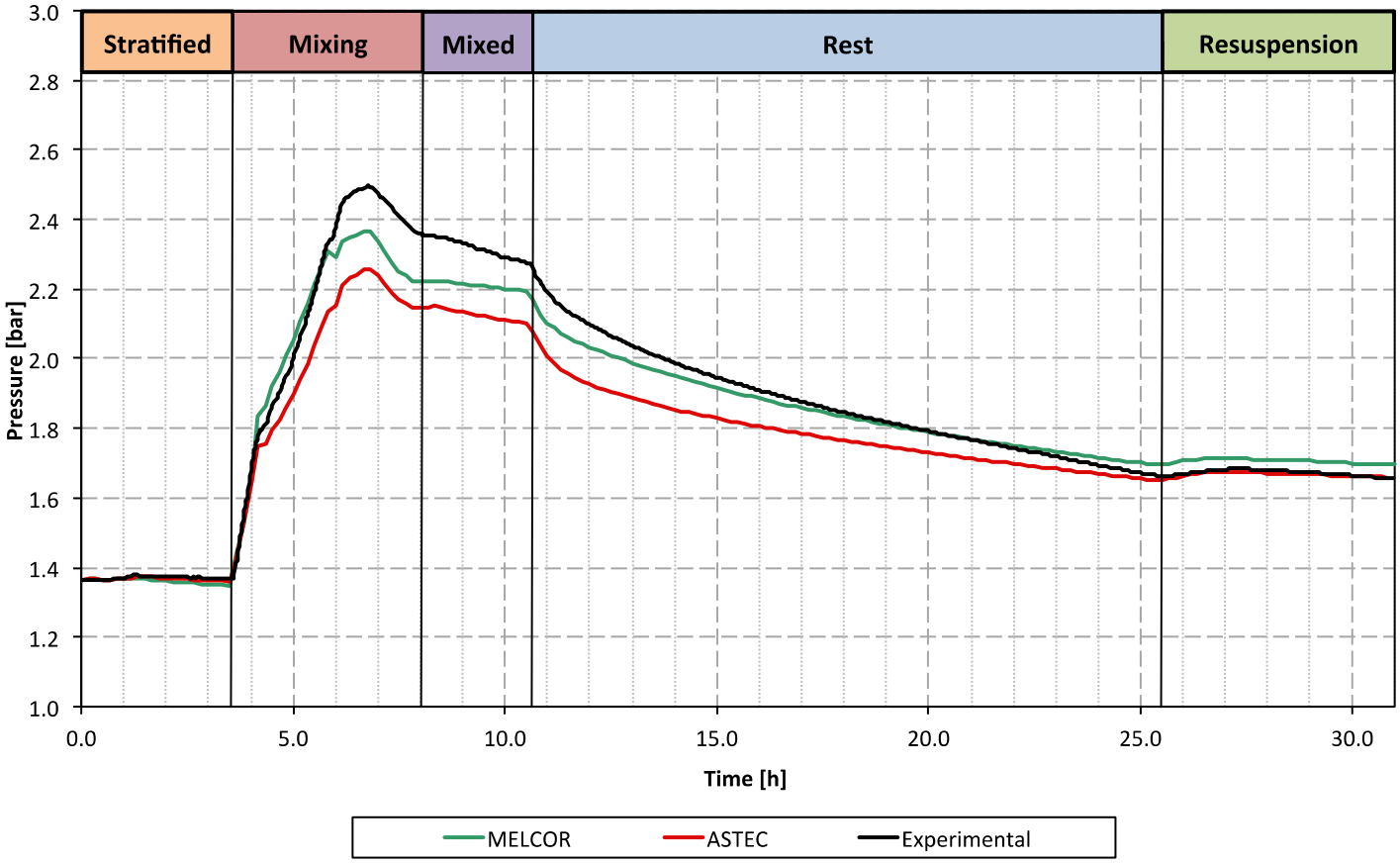

Figure 18: Total pressure in Iod-12 test.

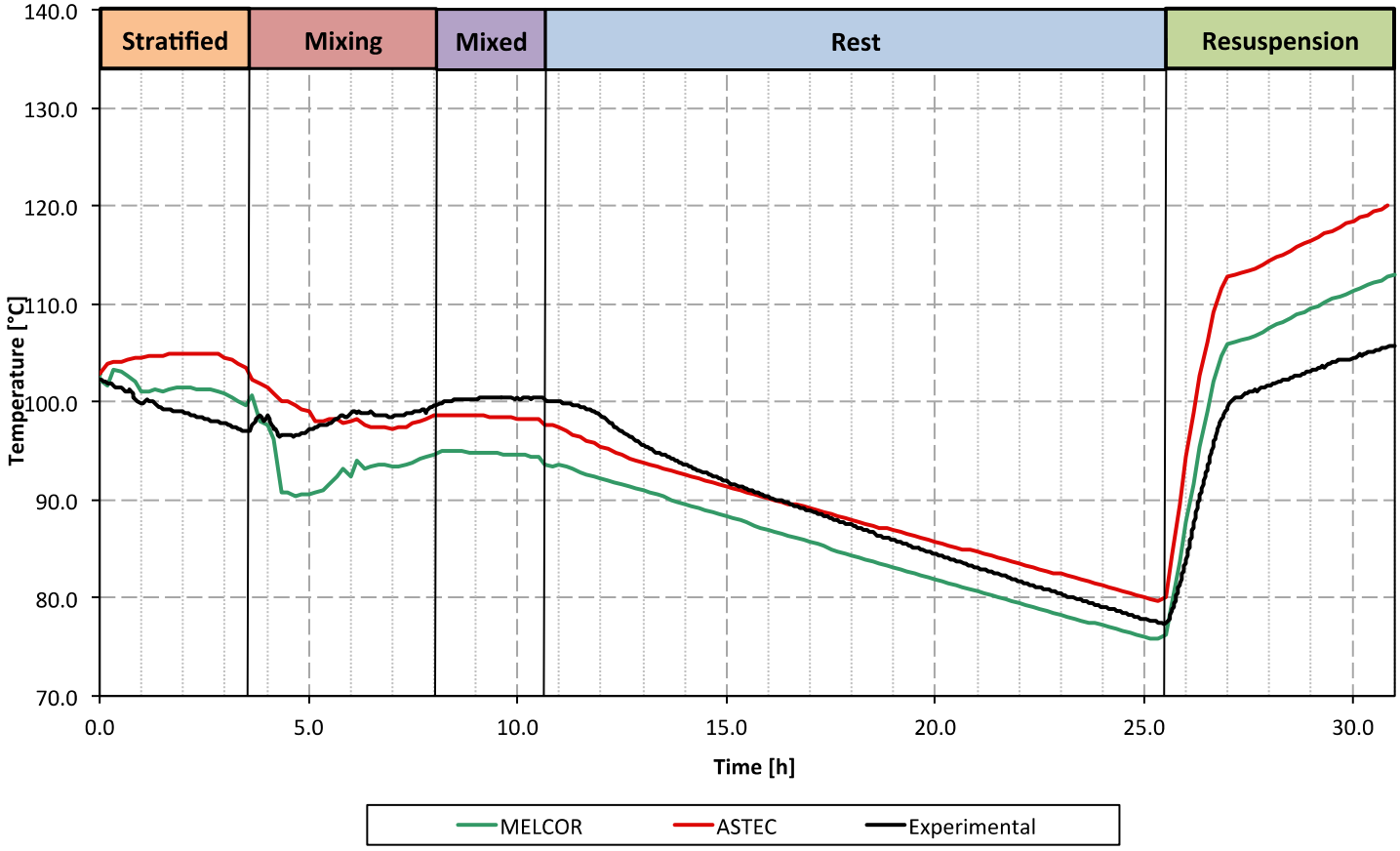

Figure 19: Atmospheric temperature in the dome compartment at 8.4 m.

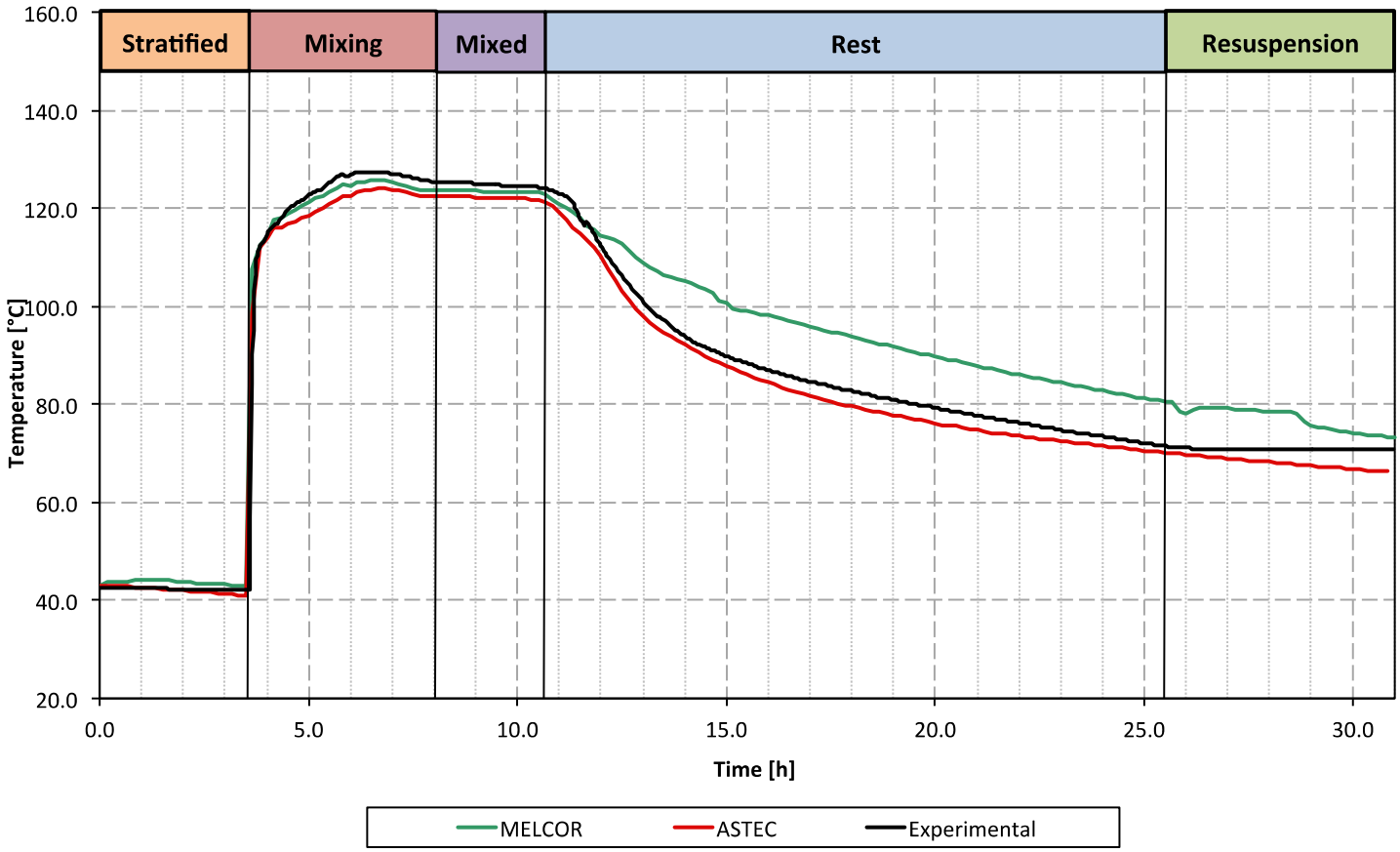

Figure 20: Atmospheric temperature in the inner cylinder compartment at 5.6 m.

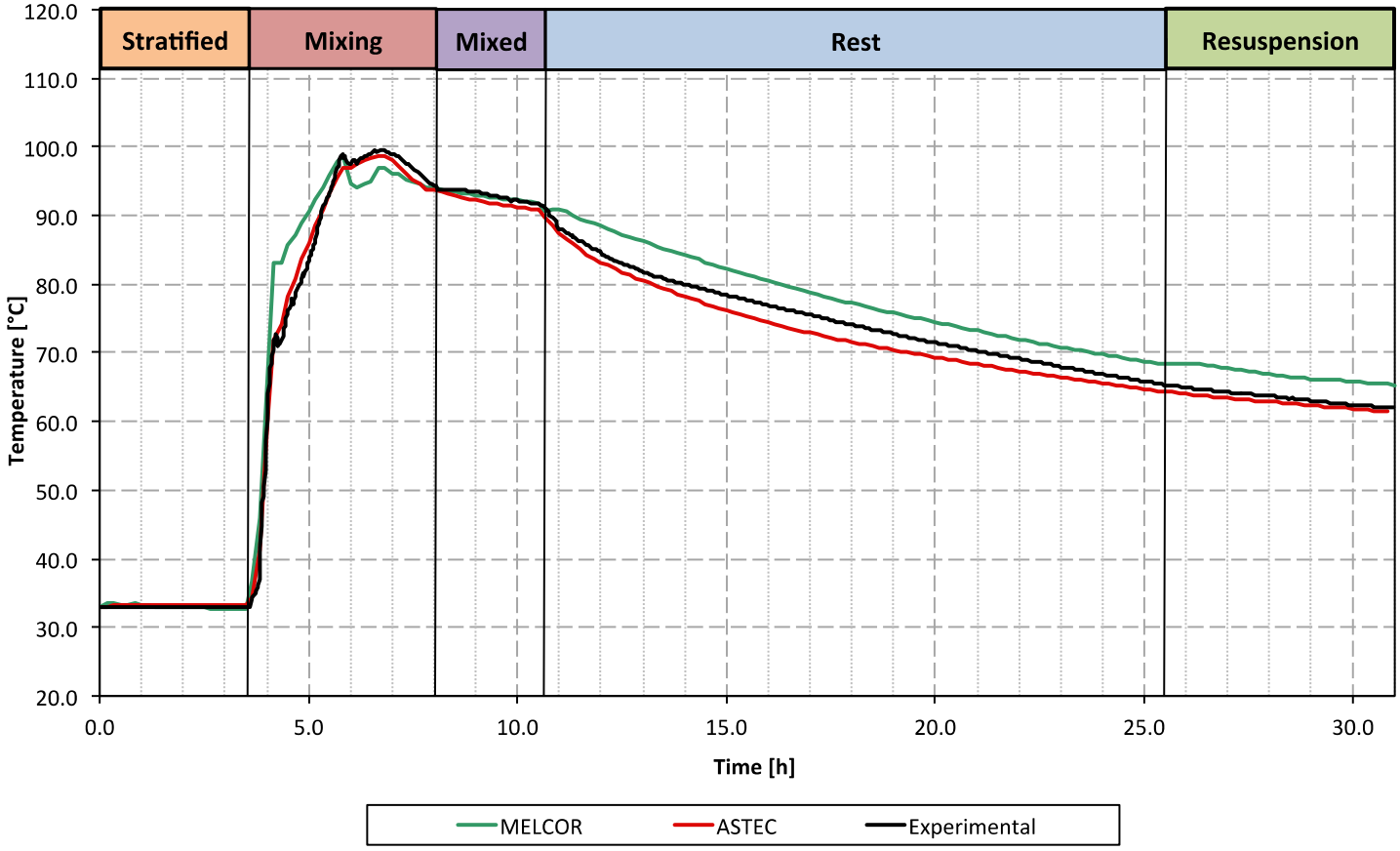

Figure 21: Atmospheric temperature in the lower annulus at 3.5 m.

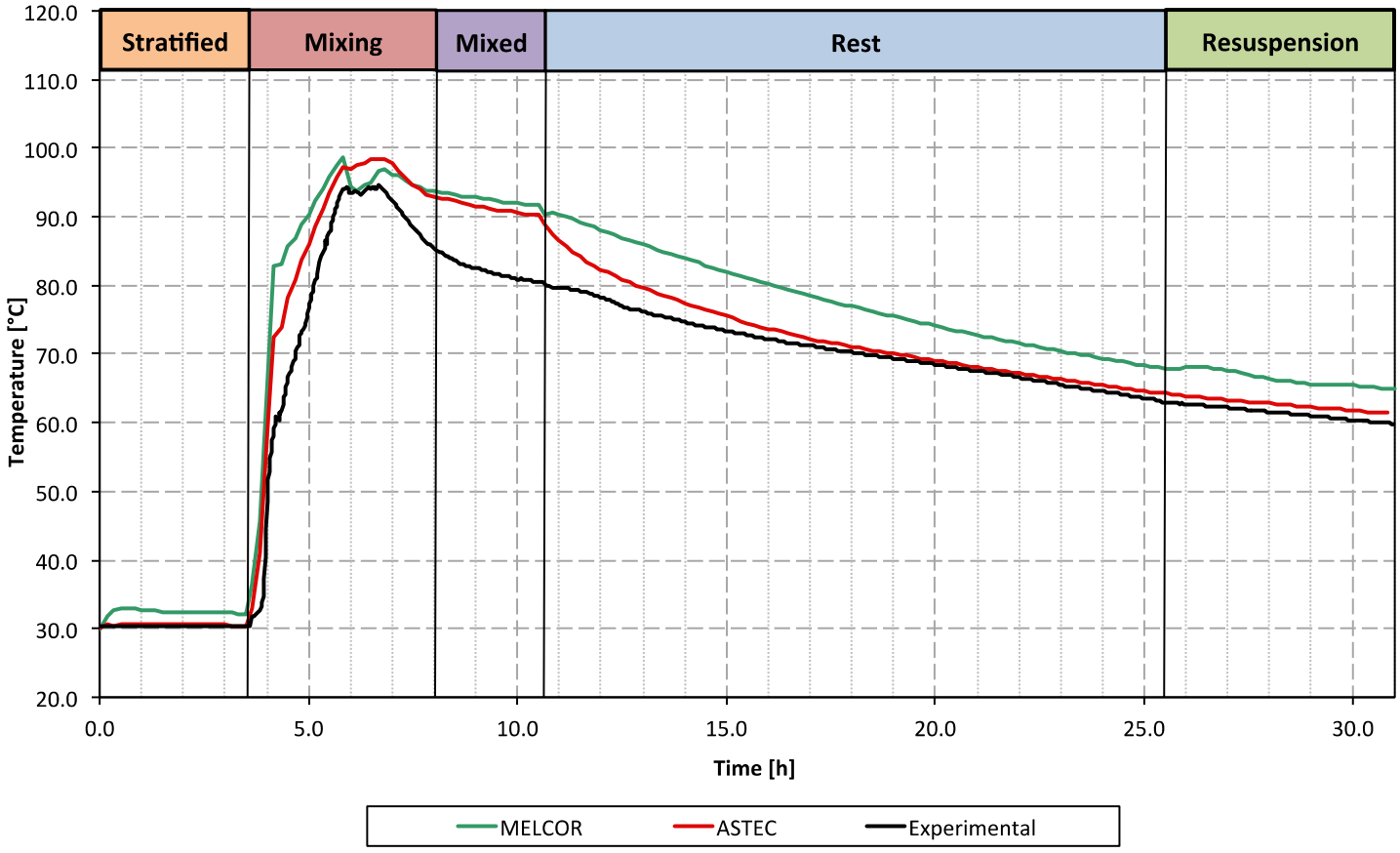

Figure 22: Atmospheric temperature in the bottom area at 2.1 m.

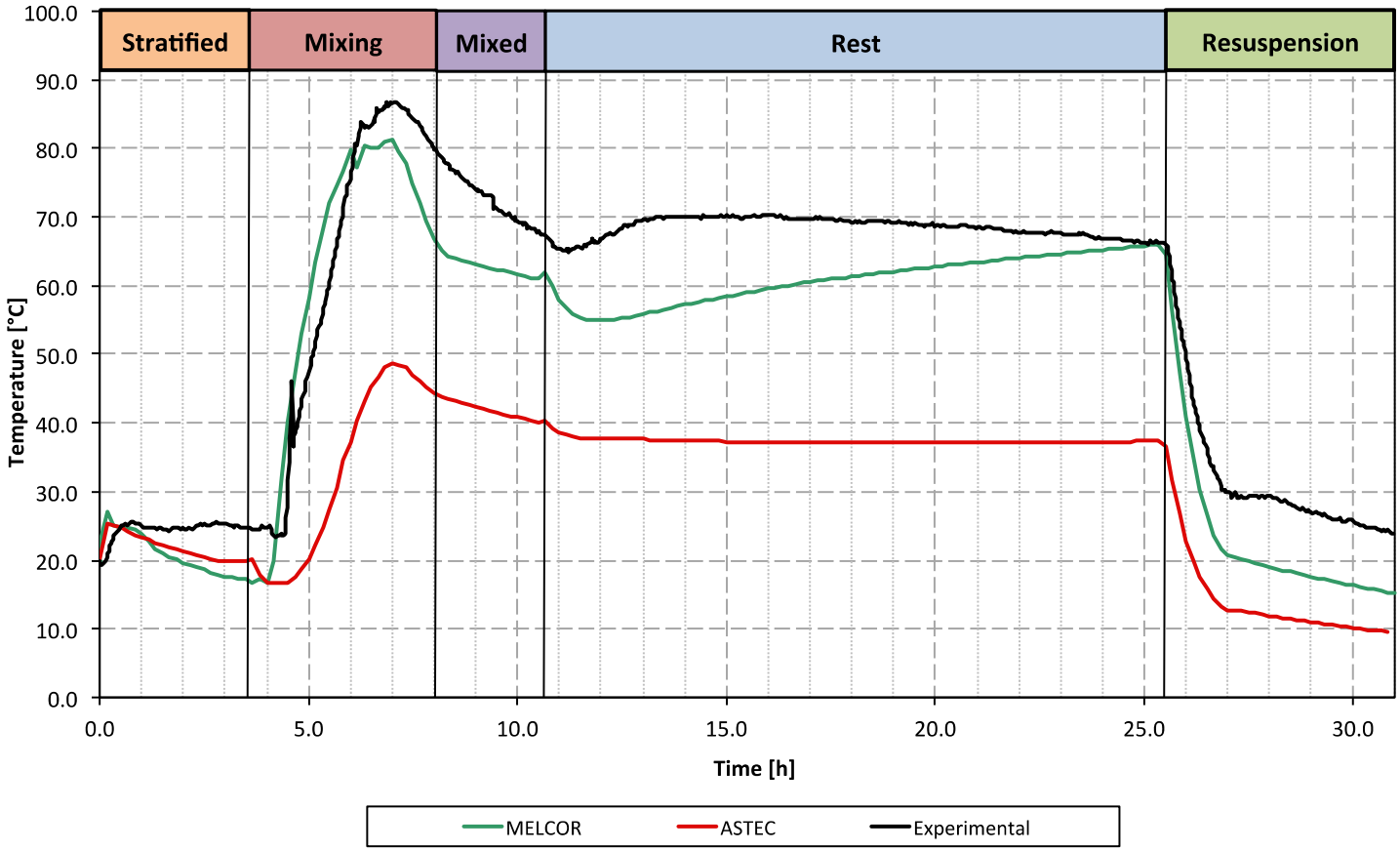

Figure 23: Relative humidity in the dome compartment at 8.4 m.

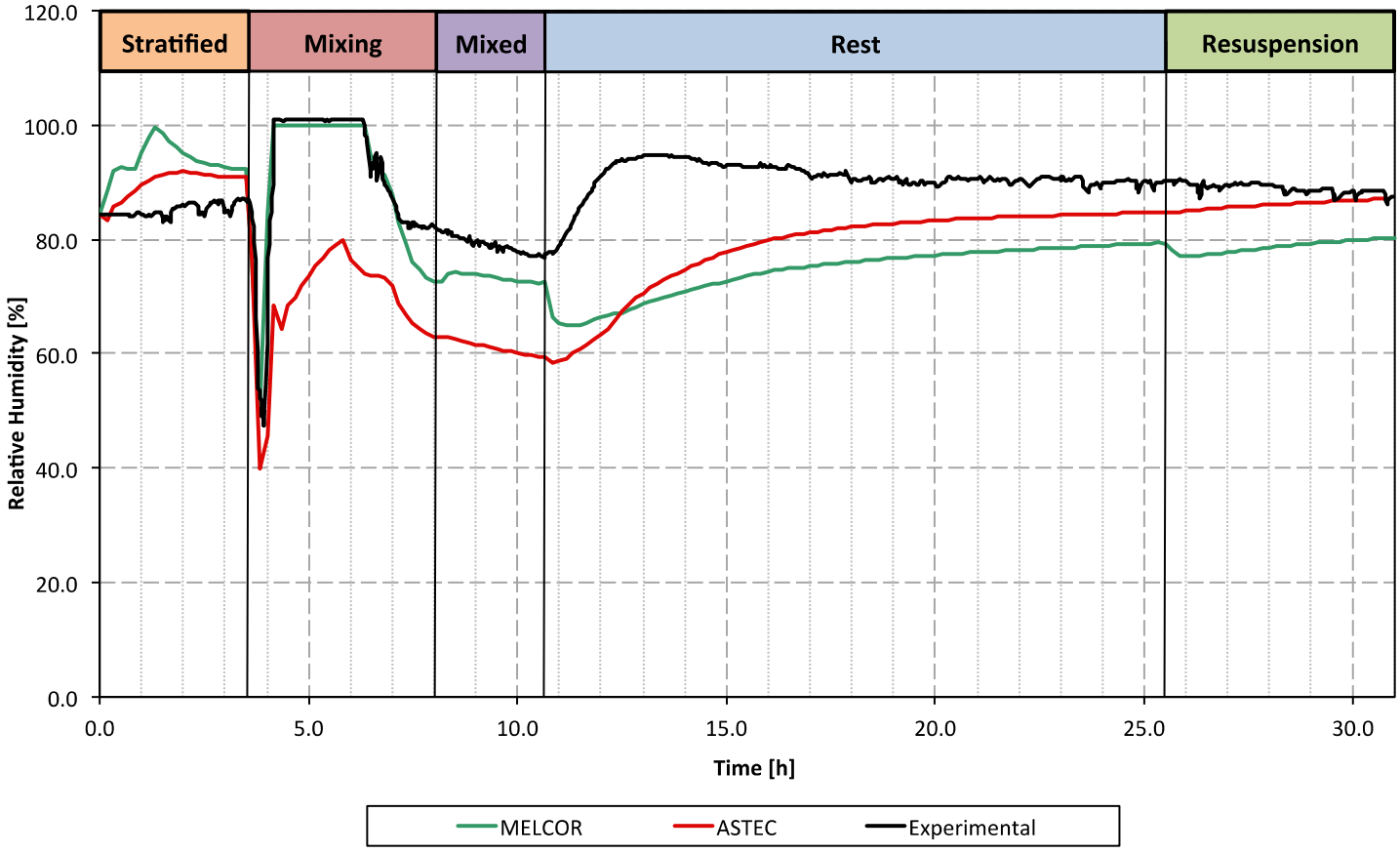

Figure 24: Relative humidity in the upper annulus at 4.9 m.

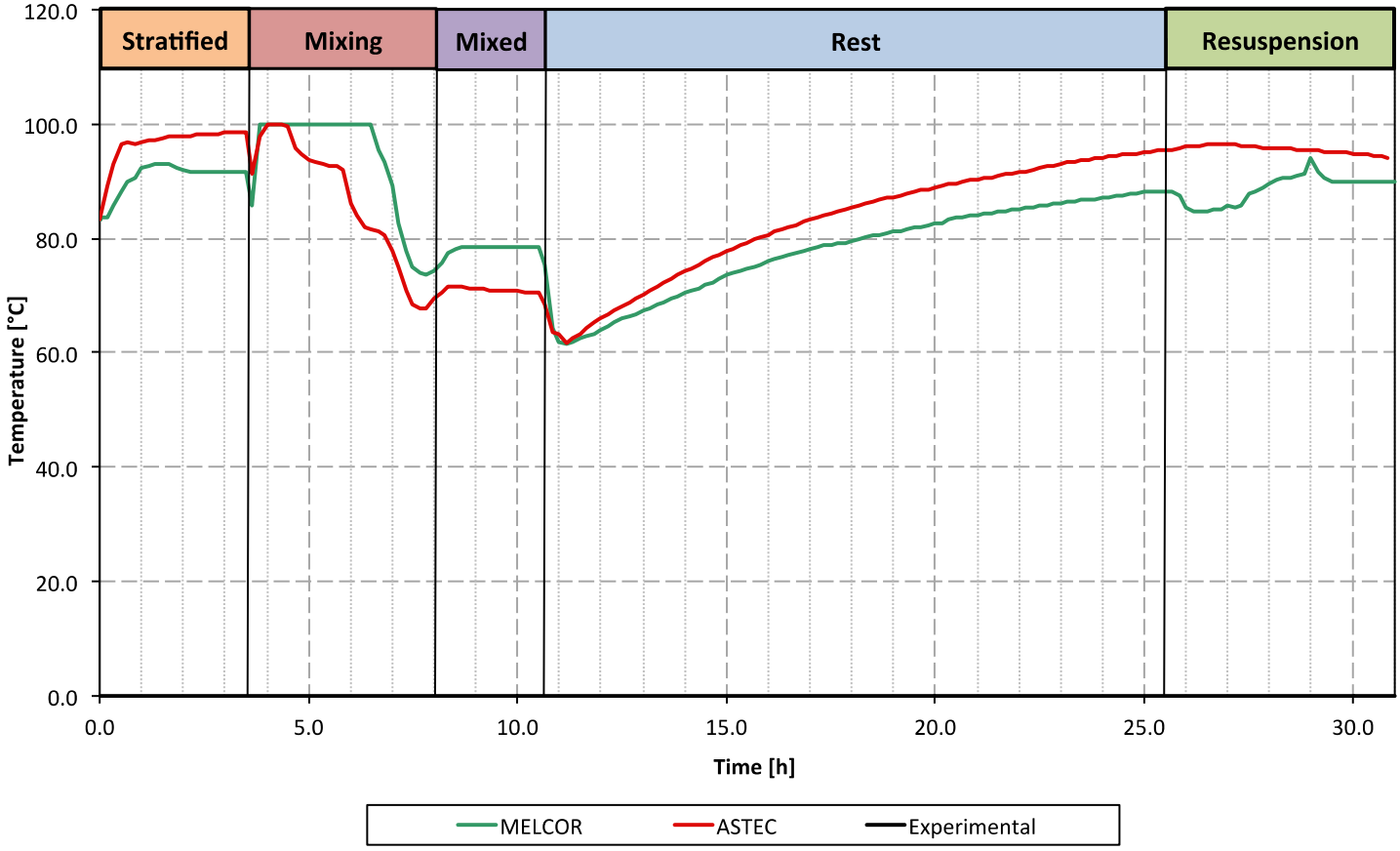

Figure 25: Relative humidity in the bottom area at 2.1 m.

The comparison among the experimental and the calculated data for the r.h. in the dome area, the upper annulus and the bottom vessel zone are reported from Fig. 23 to Fig. 25. As shown in these three graphs several differences can be highlighted, but the differences compared to the Iod-11 test seem smaller.

As shown in the figures, the stratified phase is well reproduced by ASTEC, but a slight difference can be highlighted in the upper annulus. This difference is probably due to the simulation of little mass exchanges among the vessel zones, which are not reported in the experimental data (during the stratified phase the vessel should be in stationary conditions). Following, in the mixing and the mixed phases several differences can be highlighted. The r.h. does not increase as expected in all the vessel zones due to local condensation phenomena in the inner cylinder (not reported here). The differences shown span from 40 % of the dome area to 30 % of the upper annulus (no experimental data were provided for the bottom zone, hence no comparison can be performed), although the trends reported are comparable to the experimental ones. In particular, all the discrepancies highlighted are due to the imperfect prediction of the first part of the mixing phase, when the steam injection is stronger. Finally, in the rest and the resupension phases the values and the trends reported are completely wrong. In the dome area the r.h. remains almost constant, while in the upper annulus the r.h. increases. In both these zone, the experimental data shown an initial r.h. increase (for the first two hours of the rest phase), and then a slightly decrease till the end of the test, which became very strong during the resuspension phase in the dome area due to the heat provided by the upper h/c jacket. The maximum errors shown in these phases are 30% for both the upper annulus and the dome zones, but this error tends to reduce during the resuspenion phase. At the end of the test in the dome area the r.h. is underestimated of 20%, while in the upper annulus the experimental and the calculated results are comparable, but this last reduction is obtained predicting a wrong trend.

Regarding the MELCOR code, better results are predicted but still inacceptable. In the stratified phase condensation phenomena are reported in the upper annulus, while the experimental results

report an almost constant r.h. On the contrary, in the dome area a slightly r.h. decrease is shown, thus it could be credible that part of the steam contained inside the dome area is routed toward the lower vessel zones. This hypothesis is also enhanced by the helium and the iodine concentrations, which demonstrate that a continuous mass flow from the upper to the lower zones is predicted (the helium concentrations remain higher in the bottom area, while higher iodine concentration are shown in the lower vessel zones). During the stratified phase the maximum discrepancy among the calculated and the experimental results is shown by the upper annulus (20 %, absolute value), while in the dome area is only 10 % (absolute value). Following, the mixing and the mixed phases are well reproduced, especially the mixing one. In the mixed phase some slight values differences can be highlighted, but less pronounced compared to ASTEC and the previous stratified phase. Finally, in the rest and resupension phases, a quite different trend is shown in both zones. The calculated trends are characterized by an initial r.h. decrease in the first hour of the rest phase followed by a continuous increase till the end of the rest phase. Although, the experimental trend is characterized by an initial increase followed by a slight decrease, thus it can be stated that the flow pattern inside the vessel is not well reproduced. However, at the end of the rest phase the difference among the experimental and calculated results is reduced compared to the early instants of the same phase. In the upper annulus an underestimation of 10 % is shown (absolute value), while in the dome area the calculated and the experimental values are identical. Finally, in the resuspension phase the same discrepancies shown during the rest phase continue to be reported for the upper annulus zone, while in the dome area the experimental and the calculated trends are similar. Although, the r.h. fall in the early instants of the resupension phase is slightly overestimated leading to an error of 8 % (absolute value).

As conclusion it can be stated that in ASTEC similar uncertainties were also shown in Iod-11, while in MELCOR better results are predicted compared to Iod-11. The atmospheric temperatures seem not to be main causes of these behaviours, because a good agreement was shown inside the various vessel zones, except during the rest and resupension phases in the inner cylinder. For this purpose, the only other cause can be found in the imperfect flow pattern predicted, which influences also the condensation phenomena inside the various vessel zones especially in the inner cylinder and the annulus areas. The uncertainties shown in term of r.h. could influence the iodine-steel interaction, especially in ASTEC, but thanks to the approach employed to calculate the reaction velocities this influence should be reduced (see section 7). For this purpose, it could be stated that good iodine results can be expected also if the thermal-hydraulic results are not in good agreement with the experimental ones.

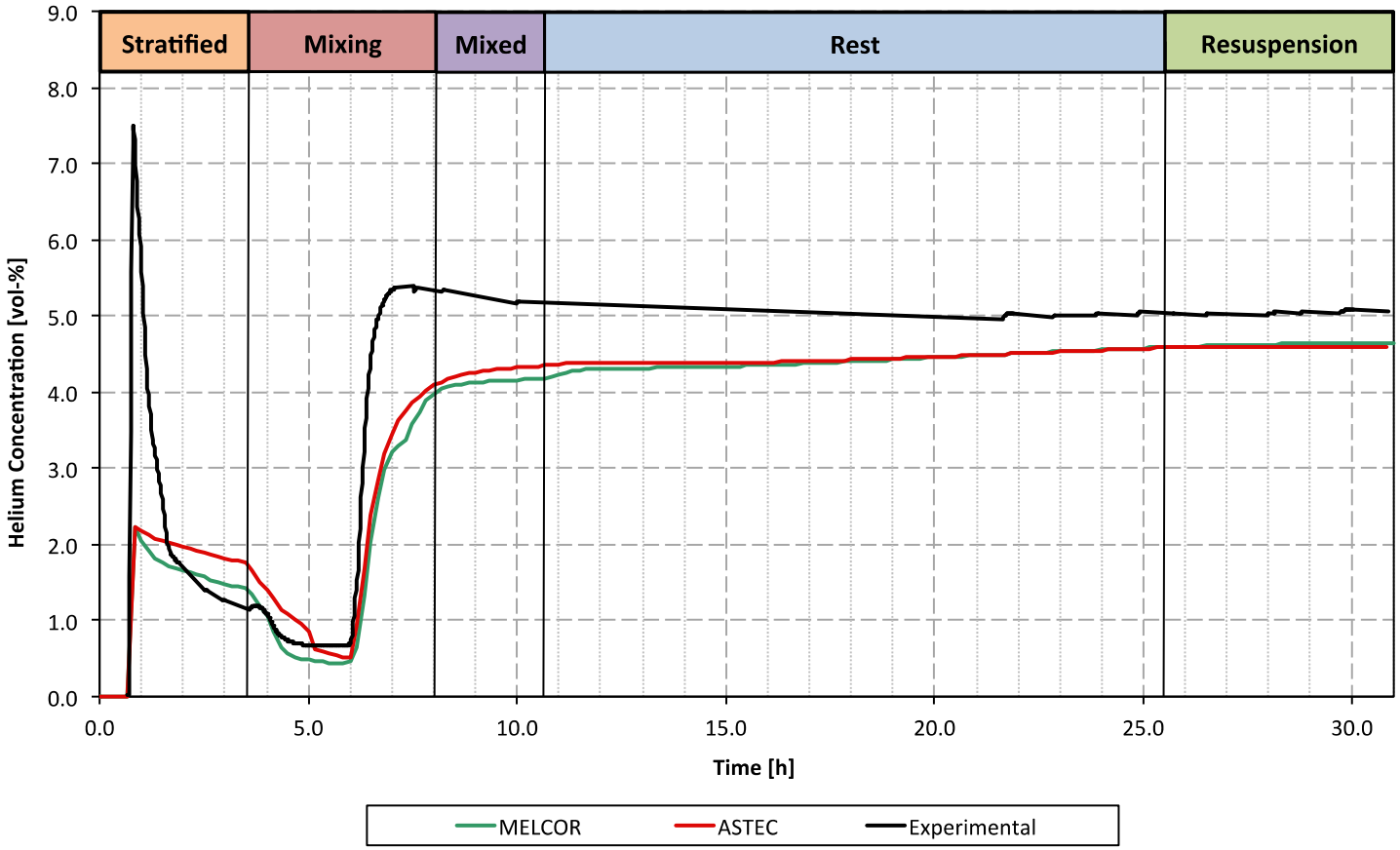

Figure 26: Helium concentration in the dome area at 8.7 m.

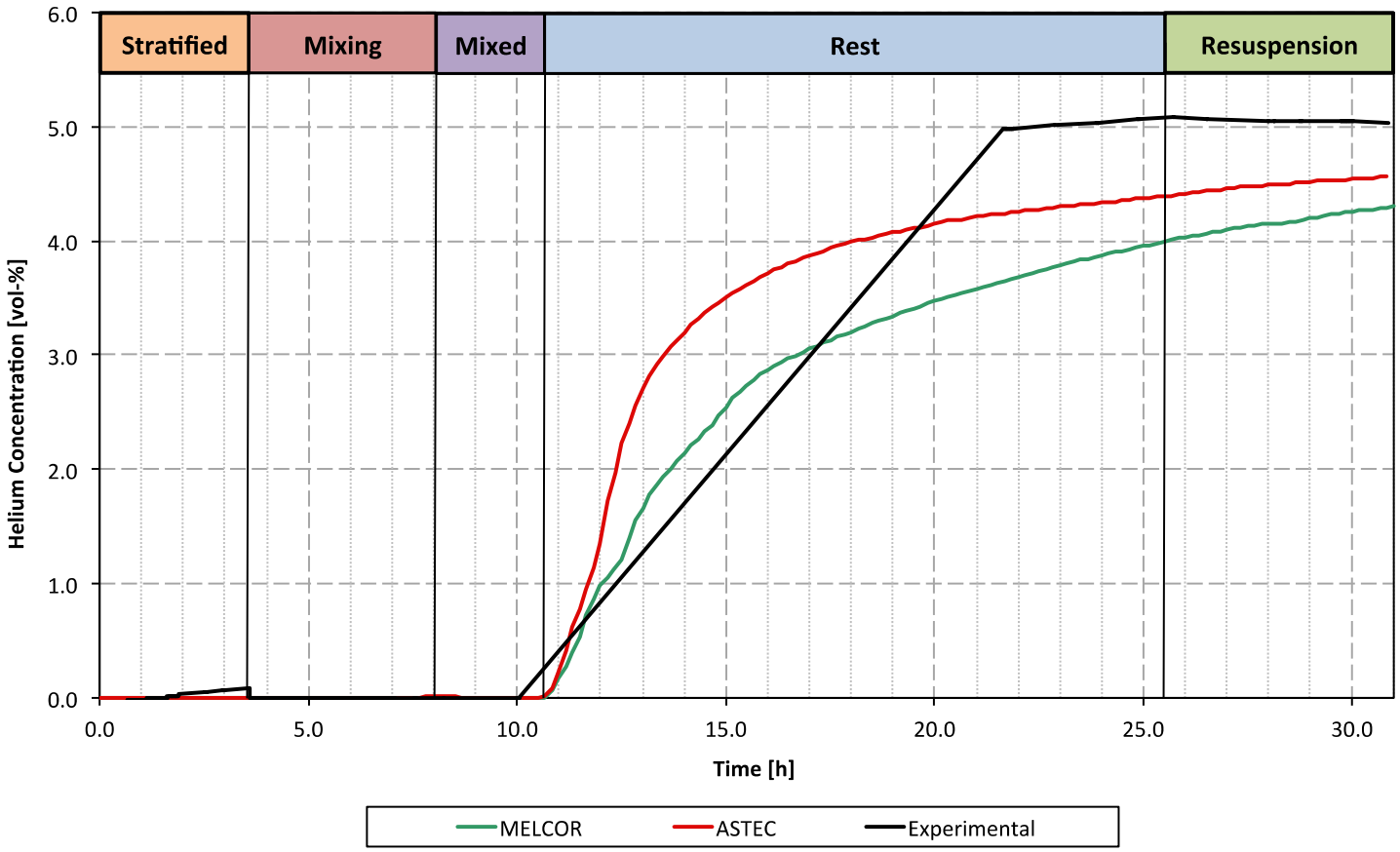

Figure 27: Helium concentration in the inner cylinder at 5.4 m.

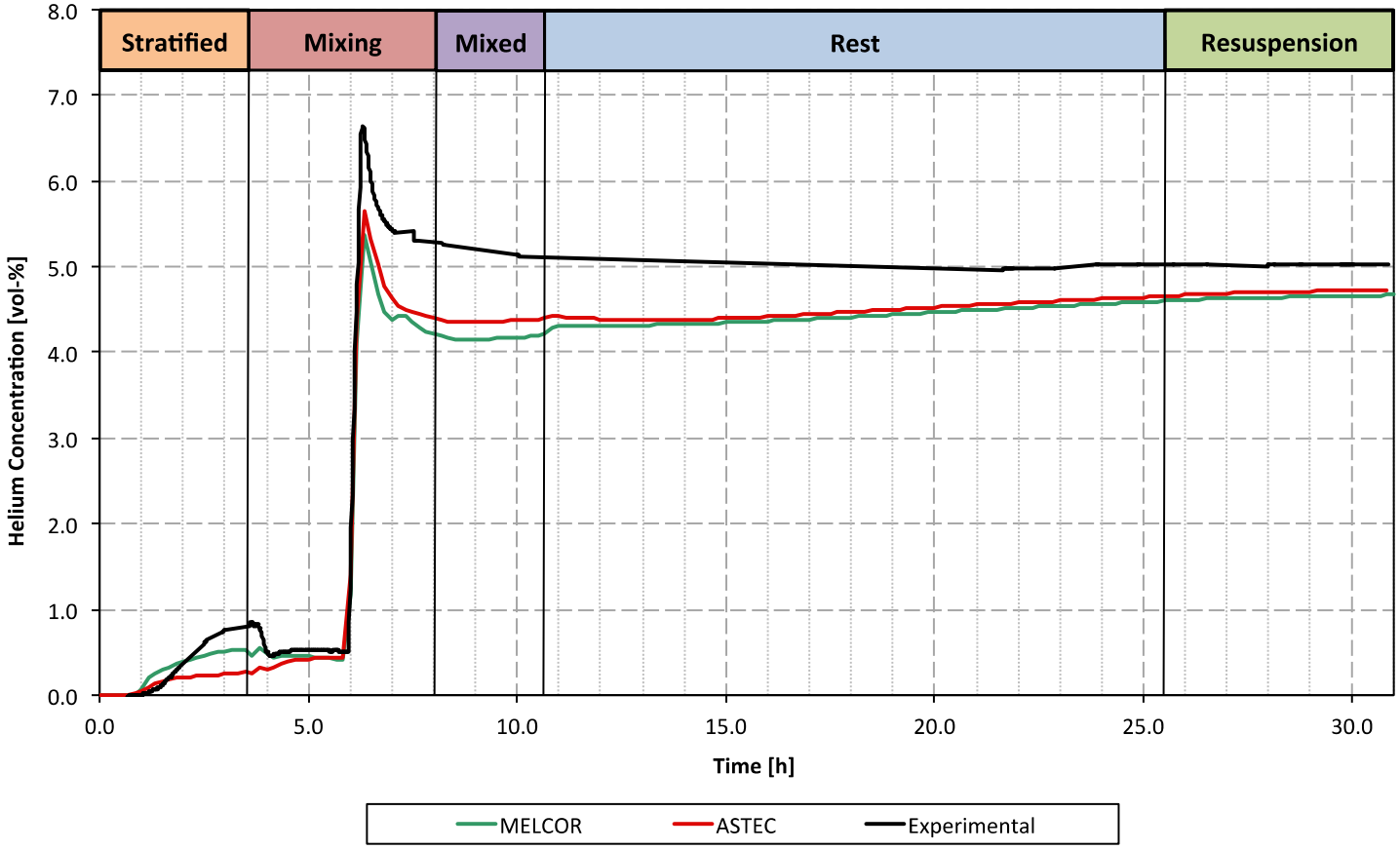

Figure 28: Helium concentration in the upper annulus at 4.6 m.

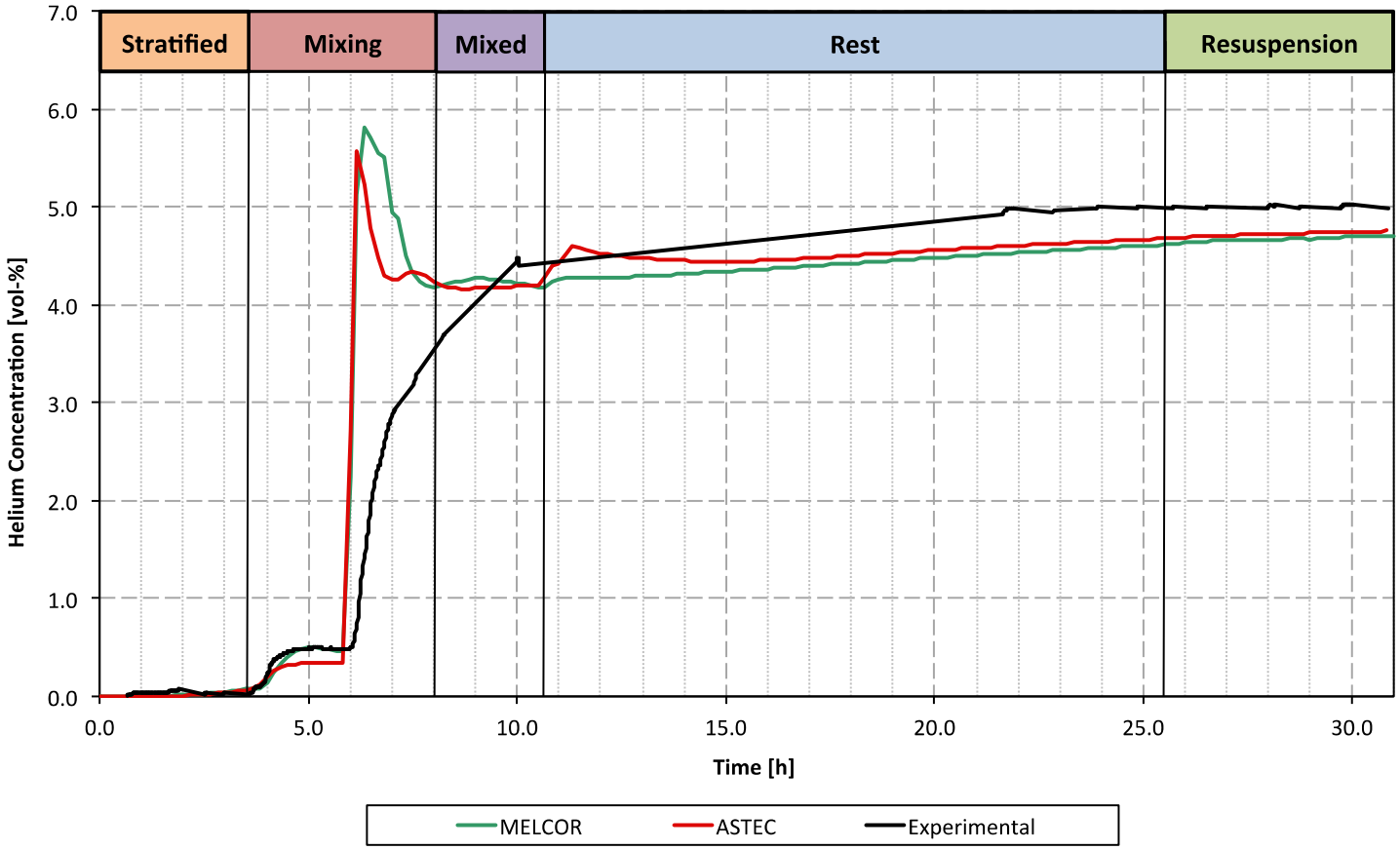

Figure 29: Helium concentration in the bottom area at 2.1 m.

From Fig. 26 to Fig. 29 the results for the helium concentrations at different heights are reported. It should be highlighted that the THAI experimental data are characterized by several uncertainties [4]. First, they refer to a steam-free atmosphere, hence the concentrations shown after 5 h are slightly

overestimated compared to the experimental values. Second, the initial peak at 8.7 m is a local effect, hence its simulation by lumped parameters codes is quite difficult. Third, the trend shown in Fig. 27 from 10 h to 21.5 h is due to the absence of experimental data during this time frame, hence the reported trend is not realistic. Therefore, the comparison between calculated and experimental data should be based on overall trends instead of a pure values comparison.

As it can be seen the two codes predict similar results. During the first 10 hours of the test the results in term of helium concentration demonstrate the hypothesis of incorrect flow pattern made for the r.h. trends. This hypothesis considers that at the beginning of the test the atmosphere is not well stratified in both codes as reported in the experimental results, hence different helium concentrations could be predicted. This incorrect prediction is then shown in the inner cylinder, the annulus and the bottom zones. In the inner cylinder the initial helium flow during the stratified phase is not reproduced, as well as the transport toward the upper annulus, which is underestimated. On the contrary, a higher than expected helium concentration is shown in the bottom area during the mixing phase. This phenomenon could be due to the fact that the helium concentration is measured inside the same volume in which the injection take place, but it cannot be excluded that an incorrect mass flow pattern prediction. For this purpose the causes of this overestimation are not clear, but as shown in Fig. 29 this event does not influence negatively the helium prediction during the final phases of the test. In particular, the helium concentration trends are slightly different from the experimental ones during the rest and the resupension phases, due to the incorrect prediction of the r.h. inside the dome and the annulus zones.

As conclusion it can be stated that the helium concentrations shown during the first 10 h of the test enhance the hypothesis of the incorrect flow pattern predicted inside the vessel. Nevertheless, the helium concentrations are in good agreement with the experimental data during the late phases of the test, thus the flow pattern are better predicted during these phases.

9.4 Iodine concentration

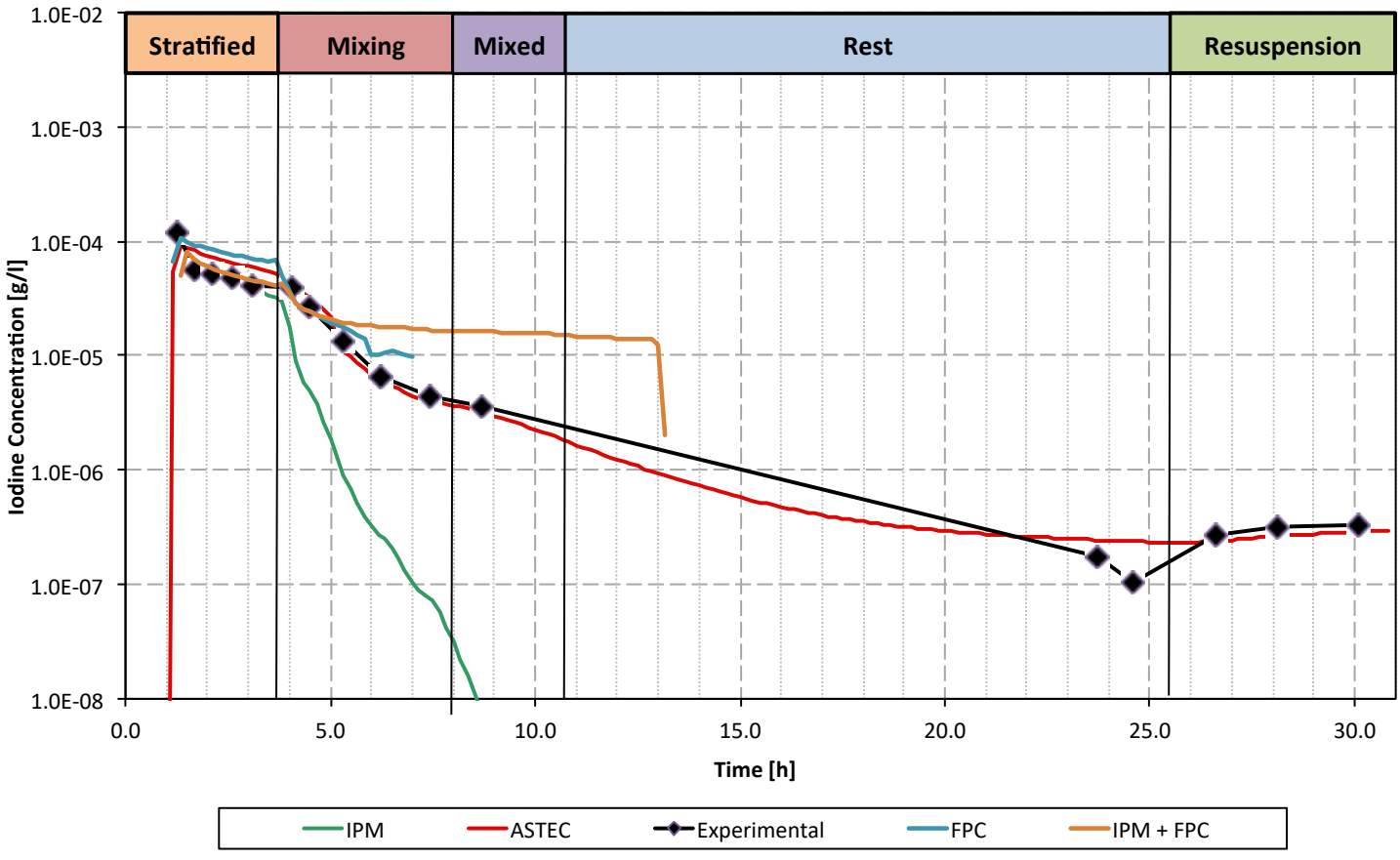

Figure 30: Iodine gaseous concentration in the dome area at 8.7 m.

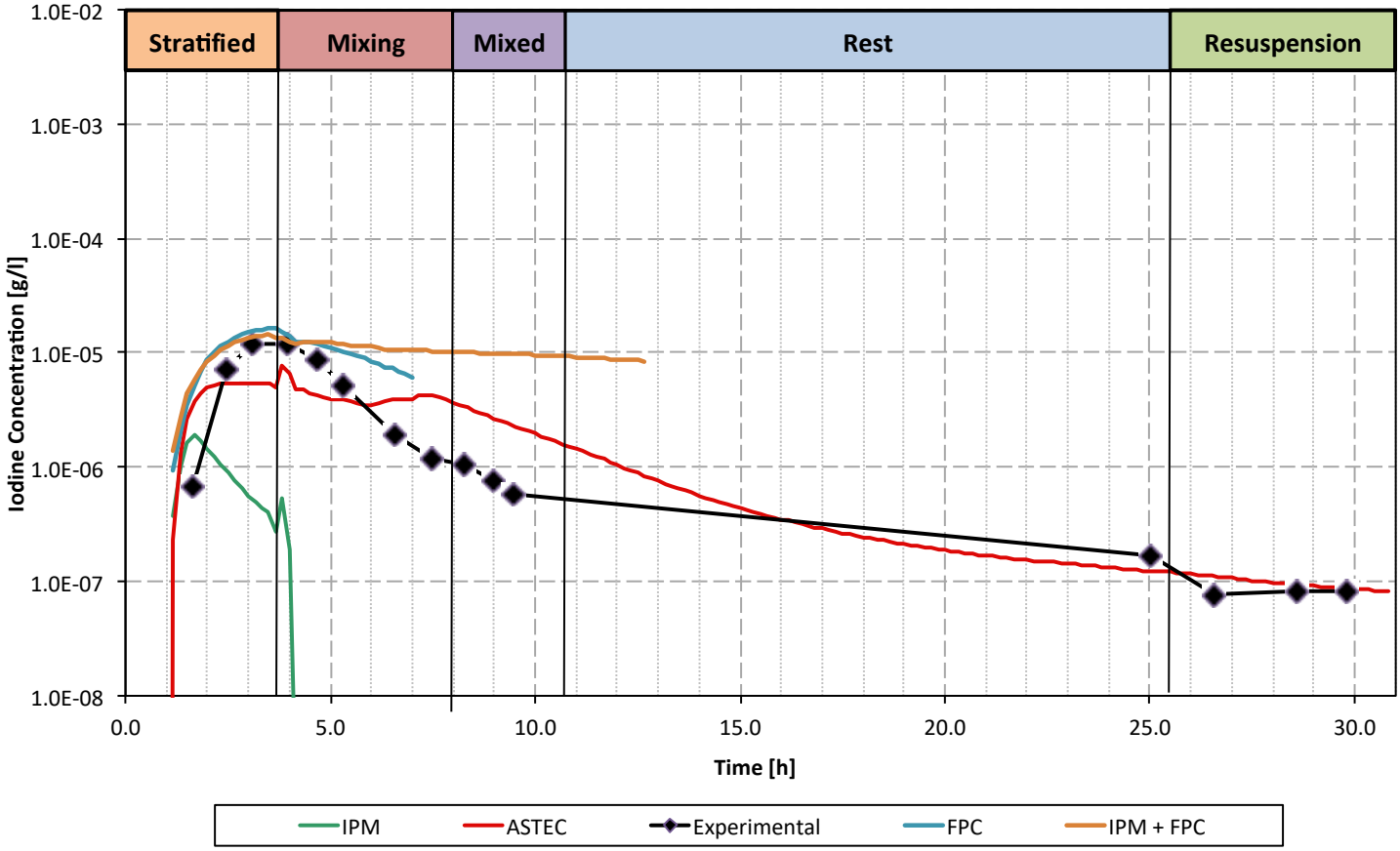

Figure 31: Iodine concentration in the upper annulus at 5.3 m.

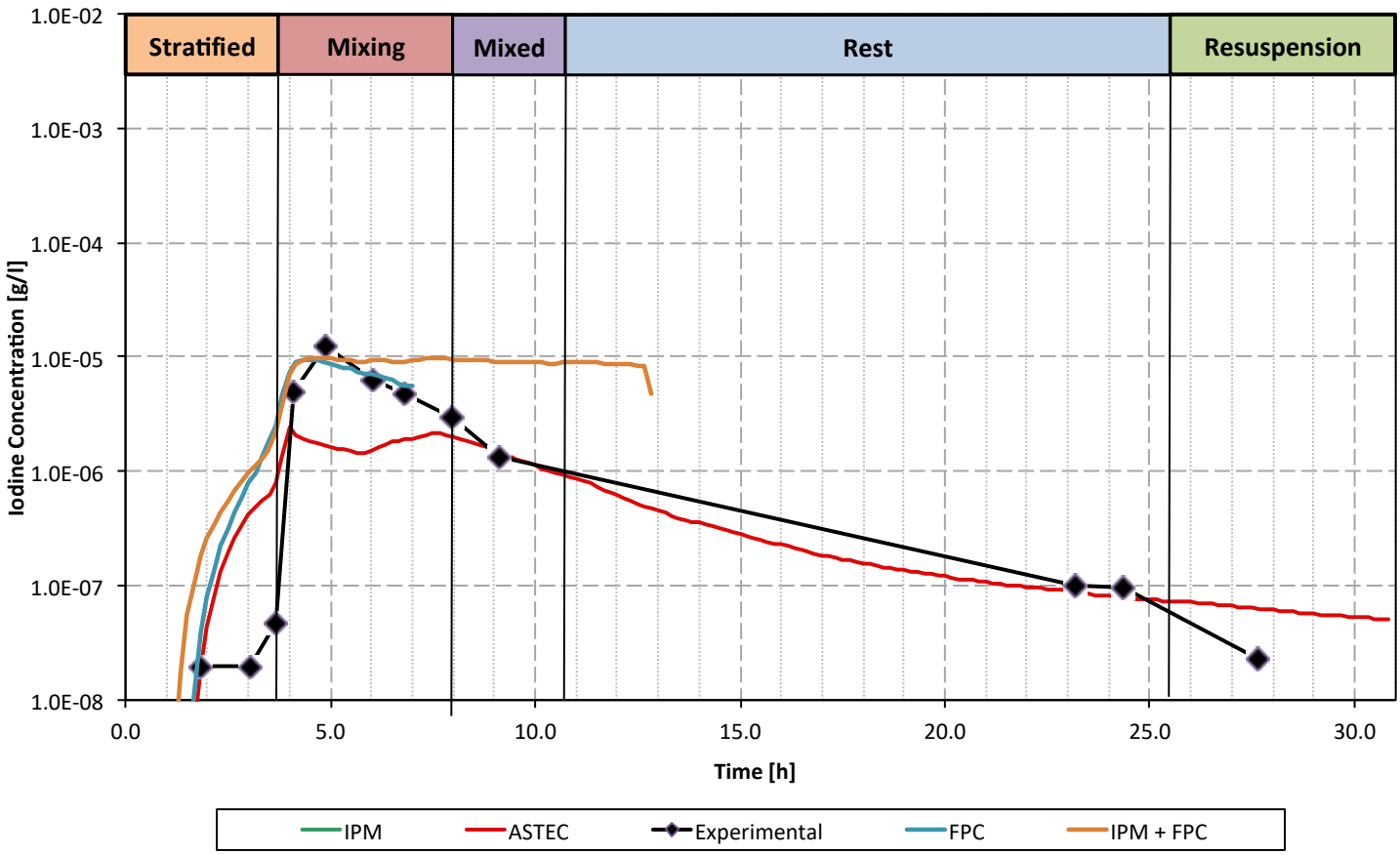

Figure 32: Iodine concentration in the bottom area at 1.8 m.

From Fig. 30 to Fig. 32 the iodine atmospheric concentrations in the dome, the upper annulus and the bottom vessel area are shown. As for Iod-11 only a single time vs reaction velocity table has been implemented for the whole vessel.

In MELCOR, during the stratified phase a quite complex behaviour is shown. In the early instants of the test the iodine concentration is well reproduced by the IP model but due to the continuous steam condensation the iodine is transported form the "aerosol" form to the "vapour" form, which cannot be computed by IP model. For this cause the iodine concentration begins an unrealistic decrease ending with the complete disappearance of iodine from the vessel.

Due to the limitation reported in the IP the FPC models was investigated. In the stratified phase a iodine redistribution toward the lower vessel zones is highlighted. During this phase the iodine concentration is overestimated of two orders of magnitude in the bottom area, and of one order of magnitude in the upper annulus. On the contrary, quite good results are shown in the dome area. At the end of the stratified phase the dome and the upper annulus zones are well reproduced (error below one order of magnitude), while in the bottom area the concentration continues to be overestimated of two orders of magnitude. This behaviour is probably due to the incorrect prediction of the flow pattern inside the whole vessel, indeed a similar behaviour was also highlighted for the helium concentrations.

Following, during the mixing phase, the code stopped to work reporting numerical errors. These errors were provided by several HSs, which were not able to calculate the mass transfer coefficient for the process. For this purpose several HSs were deactivated but the errors were not solved, thus the investigation on the FPC model was stopped. For this purpose the joint activation of the IP and FPC models was executed. The analyses carried out with this option were characterized by an almost constant prediction of the iodine concentration in the mixing and the mixed phases, while in the experimental results a continuous decrease is reported. Finally, numerical errors were provided during the rest phase as in the stand-alone FPC model run.

On the contrary, the ASTEC code predicts good results during the test, except in the stratified and the mixing phases where a quite faster redistribution toward the lower vessel zones was reported. In the experimental results, the iodine concentration peak is reported at 4.0 h in the annulus zone and at 5.0 h in the bottom area, meaning that iodine is slowly pushed toward the lower vessel zones. After this initial redistribution a continuous concentration decrease is shown in all the vessel zones due to its deposition onto steel surfaces. In ASTEC this complex behaviour is not shown because the flow pattern and the iodine-steel interaction seem not well reproduced. A quite large part of the iodine injected in the dome is rapidly routed toward the lower vessel zones, leading to higher concentrations in both the annulus and the bottom vessel zones.

In the mixing phase a quasi-constant concentration is reported due to the insufficient iodine-steel reaction velocity. However, at the end of the mixing phase the iodine concentration shown by the bottom area is comparable with the experimental one, while in the upper annulus an overestimation of around 5 g/l is reported.

In the mixed and the rest phases of the test the dome and the bottom vessel areas reproduce perfectly the iodine behaviour, while in the upper annulus a stronger iodine-steel interaction is reproduced. Finally, in the resuspension phase good results are shown in all the vessel zones, except in the bottom area where a slight concentration overestimation of 3.0E-8 g/l is reported.

As conclusion it can be stated that two codes provides completely different results, and also several differences compared to the Iod-11 tests can be highlighted. ASTEC predicts good results but the initial incorrect flow pattern leads to improper iodine concentration in the first 10 h of the test, while in MELCOR modelling problems affect the calculation. For this purpose it can be stated that the IP and the FPC models are not able to predict the iodine behaviour, hence only the chemisorption model can be employed to simulate iodine [4]. Nevertheless, this model is not able to reproduce the complex reactions involving iodine [3] so, in the future, the IP model should be expanded to cope also with the "vapour" form, or a new model should be introduced.

10 Extension to ASTEC v2.0R3p2 and MELCOR V2.1.6342

During the final phases of this work two new versions were released for both ASTEC and MELCOR. For this purpose some analyses were carried out also with these new versions to underline new improvements or lacks related to the iodine modelling. The key aspect of this analyses can be listed as follow:

- Regarding the MELCOR code a new issue was found in the IP model during the input deck check phase due to some unexplained errors. After several analyses the problem was found in the card employed to define the CVs taking part to the IP model. In particular the activation of the card was the problem, not the CVs itself. To solve this error a partial reconstruction has been performed but the problem was not fixed. The problem is probably due to the complex input deck employed, and in the future further detailed analyses should be executed to solve this error.
- Regarding the FPC model the same problem of the V2.1.4803 version was found, hence
- On the contrary, the new ASTEC version provided similar results compared to the older one (R3p1).

As conclusion it could be stated that in MELCOR the new version seems to include new bugs compared to the previous one, while in ASTEC no major differences can be highlighted among the two versions.

11 Conclusions

The aim of this work was to re-evaluate the capabilities of the ASTEC and the MELCOR codes to simulate two of the main benchmark exercises focusing on the iodine-steel interaction. For this purpose the THAI Iod-11 and Iod-12 tests were selected thanks to their complexity and the deep coupling between thermal-hydraulic and iodine behaviour. To stress the differences among the two codes the following choices were also employed:

- A similar nodalisation was employed in both codes. This nodalisation was mainly built basing on the geometric characteristic of the vessel and on the tips provided in the benchmark specifications [4].
- The outer environment temperature was set to 20 °C in both codes and in ASTEC the outer heat exchange coefficients was also set to 20 W/m^{2}K. This last boundary condition was not introduced in MELCOR due to the intrinsic limitations of the input deck.
- The iodine-steel interaction was simulated imposing two tables containing the reaction velocities for both the adsorption and the desorption reactions. This is the approach required by ASTEC, but for MELCOR also user correlation could be introduced, but due to the intention to employ similar nodalisations this MELCOR capabilities was not tested. Moreover, in MELCOR different models were investigated to solve the problems shown during the Iod-12 test.
- An initial steady-state calculation was not performed due to difficulties to obtain correct initial vessel conditions.

Comparing this work with the SARNET benchmark the following two differences can be stressed:

- In the SARNET exercise only the older MELCOR 1.8.x versions were employed, while in this work the new 2.1 version was employed.
- In this work an identical nodalisation is employed in both codes, hence the differences reported among the two codes are due to their different nodalisation interpretation. For this purpose this work allows a comparison 1:1 among the capabilities of the two codes, while in the SARNET exercise the comparison among different codes was difficult to perform due to the different nodalisation employed by each participant.

In Table 6 a comparison among the results shown in this work and in the SARNET exercise [4] are reported.

Table 6: Comparison among the results shown in this work and in the benchmark exercise.

Test	Parameter	Comparison	
		ASTEC	**MELCOR**
Iod- 11	Total pressure	The results shown are slightly better compared to the benchmark exercise ones.	The results shown are comparable with the benchmark exercise ones.
	Atmospheric temperature	Similar results were shown in the benchmark exercise, except in the stratified phase where lower differences were highlighted.	In the benchmark exercise the results were closer to the experimental data compared to the analyses here carried out.
	Relative humidity	In the benchmark exercise quite different results were shown but yet comparable with the experimental ones, while in the present work the differences shown are too high. On a numerical point of view the differences are similar, but comparing the overall trends several differences are highlighted.	
	Helium concentration	In this work, except for the inner cylinder zone, the helium concentrations are better predicted compared to the benchmark exercise.	
	Iodine concentration	Better results are shown compared to the benchmark exercise ones.	The IP model results are comparable with the benchmark exercise ones, but improved thermal-hydraulic results will be also beneficial for the overall IP model behaviour.
Iod-12	Total pressure	The results shown are comparable or better than the benchmark exercise ones.	
	Atmospheric temperature	Better results were shown for the dome area compared to the benchmark exercise ones, while for the bottom area similar discrepancies were shown.	
	Relative humidity	The results shown are completely different compared to the experimental and the benchmark exercise ones.	The results shown are slightly better than the benchmark exercise ones.
	Helium concentration	The results shown are comparable with the benchmark exercise ones.	
	Iodine concentration	Better results are shown compared to the benchmark exercise ones.	The extended condensation phenomena make the IP model unsuitable for the analysis of this test. For this purpose also the FPC model was investigated but the numerical issues experienced do not allow their application to complex tests.

On the thermal-hydraulic point of view it can be stated that both codes are able to simulate the Iod-11 and Iod-12 transients, but some discrepancies are shown. These discrepancies are mainly due to the incorrect flow pattern prediction during the stratified and the mixing phase in both tests. The difficulties to reproduce this flow pattern are linked to the different temperatures show in the upper annulus and lower dome zone at the beginning of the tests. In detail, the dome temperature is higher

than the upper annulus one, and the structures dividing these two zones are characterized by a strong temperature gradient. Moreover, also the lower outer dome structure (below the upper h/c jacket) is colder than the dome, thus from 6.3 m to 6.5 m a quite complex temperature distribution is reported. For this purpose the following points should be stressed:

- The user's guidelines of both codes were followed, but the connection among CV centres seems suitable only for pipes, while for "open" CVs short connections among the CV boundaries should be introduced. This approach was also employed in the UNIPI ECART calculation for the benchmark exercise and somewhat better results were shown [4].
- The nodalisations should not be focused only on the geometric features of the system, but also on the phenomena investigated.

These two aspects are of main importance also for real containment building. In detail a containment nodalisation should be than characterized by a sufficient higher CVs number, the shape and the dimensions of these CVs should not be based only on geometric features, and the atmospheric junctions should connect the boundaries of such CVs instead of their centres.

Regarding the iodine behaviour it can be stated that only ASTEC is able to reproduce the overall behaviour, but the imperfect thermal-hydraulic conditions characterizing the early phases of the tests provide a source of uncertainties. The early phases of the tests are characterized by a deep coupling between thermal-hydraulic and iodine, thus the imperfect simulation of the thermal-hydraulic has a direct influence on the iodine behaviour. The main parameters linking these two aspects are: the atmospheric temperature, the relative humidity and the flow pattern among the various vessel zones. The first two parameters directly influence the iodine-steel interaction, while the flow pattern influences the mass redistribution inside the various vessel zones. On the contrary, in the late phases of the tests this coupling is less pronounced and the iodine behaviour could be better predicted also if the thermal-hydraulic results are not closer to the experimental ones.

However, in this work, only the flow pattern links these two aspects because the reaction velocities introduced inside the input decks were calculated basing on the experimental conditions instead on the predicted conditions. This limitation was introduced to avoid the two-step process needed in ASTEC to calculate the reaction velocities:

- In the first step only a thermal-hydraulic run should be performed and, basing on the results obtained, the iodine reaction velocities should be calculated according to the equation reported in section 7.
- Following, in the second step the reaction velocities should be introduced in the input deck to run a coupled CPA-IODE simulation.

This approach doubles, at least, the time needed to run each simulation and become an iterative problem if the results of the IODE module influence also the results of the CPA module.

For these purposes, in the future the capabilities of the IODE module could be extended implementing the capability to introduce in the input deck the k_0 parameter and the activation energy to be employed in the Arrhenius equation. With this approach the user will be able to model the iodine behaviour with an equation drawn for the thermal-hydraulic conditions expected in its specific case instead of the common equation implemented in the ASTEC code [13].

This approach described above can be already employed in MELCOR thanks to the control function package, but it was not used because one of the main scopes of this work was to compare 1:1 the two codes. Although, several bad remarks can be also highlighted for the MELCOR code due to the several uncertainties shown by the models employed. For Iod-11 the IP model seems suitable to simulate the test, but for Iod-12 the extended condensation occurring in the vessel compromises the IP model results. For this purpose also the FPC model was investigated but several numerical issues were experienced. Several sensitivity analyses were carried out to solve these problems but no solutions were found. Therefore, as conclusion it can be stated that the IP and the FPC models are not suitable for the

iodine analyses in case of condensation phenomena, while in dry conditions the IP model seems able to reproduce all the reactions involving iodine. However, it should be also highlighted that in MELCOR also the chemisorption model can be used to simulate the iodine behaviour. The chemisorption allows the simulation of a continuous deposition onto surfaces, thus it is not able to reproduce the complex reactions involving iodine and for this cause it was not employed in the present work.

To conclude it can be stated that the iodine modelling suffers several uncertainties in both codes. In ASTEC the IODE module is able to correctly simulate complex scenarios but their capabilities could be enhanced. In MELCOR several numerical uncertainties affect the various models implemented, especially the FPC models, hence in the future these problems should be solved.

12 References

[1] B. Clément, L. Cantrel, G. Ducros, L. Herranz, A. Rydl, G. Weber e C. Wren, «State of the Art Report on Iodine Chemistry,» 2007.

[2] A. M. Beard, P. J. Bennet, C. G. Benson, C. J. Bryan, C. C. Kemp, A. V. Morton, M. S. Newland e A. P. Smith, «Fission Product Vapour - Surface/- Aerosol Interactions: Summary Report,» 1005.

[3] J. C. Wren e G. A. Glowa, «Kinetics of gaseous iodine uptake onto stainless steel during iodine-assisted corrosion,» *Nuclear Technology,* vol. 133, pp. 33 - 48, January 2001.

[4] G. H. L. E. Weber, M. Bendiab, J. Fontanet, F. Funke, B. Gonfiotti, I. Ivanov, S. Krajewski, A. Manfredini, S. Paci, M. Pelzer e T. Sevon, «Thermal-hydraulic - Iodine chemistry coupling: Insight gained from the SARNET benchmark on the THAI experiments Iod-11 and Iod-12,» *Nuclear Engineering and Design,* vol. 265, pp. 95 - 107, December 2013.

[5] J. P. Van Dorsselaere, A. Auvinen, D. Beraha, P. Chatelard, C. Journeau, I. Kljenak, A. Miassoedov, S. Paci, T. W. Tromm e R. Zeyen, «The European Research on Severe Accidents in Generation 2 and 3 Nuclear Power Plants,» *Science and Technology of Nuclear Installations,* vol. 2012, pp. 1 - 12, 2012.

[6] G. Weber, L. Bosland, F. Funke, G. Glowa e T. Kanzleiter, «ASTEC, COCOSYS, and LIRIC Interpretation of the Iodine Behaviour in the Large-Scale THAI Test Iod-9,» *Journal for Engineering for Gas Turbines and Power,* vol. 132, 2010.

[7] L. Bosland, G. Weber, W. Klein-Hessling, N. Girault e B. Clement, «Modeling and Interpretation of Iodine Behaviour in Phébus FPT-1 Containment with ASTEC and COCOSYS codes,» *Nuclear Technology,* vol. 177, pp. 36 - 62, 2012.

[8] L. Bosland, L. Cantrel, N. Girault e B. Clement, «Modeling of Iodine Radiochemistry in the ASTEC Severe Accident Code: Description and Application to FPT-2 Phébus test,» *Nuclear Technology,* vol. 171, n. 1, pp. 88 - 107, 2010.

[9] OECD/NEA, «THAI Prokect Hydrogen and Fission Product Issues Relevant for Containment Safety Assessment under Severe Accident Conditions,» OECD, 2010.

[10] H. Nowack, N. Reinke e M. Sonnenkalb, «Continuous validation of ASTEC containment models and regression testing,» *Nuclear Engineering and Design,* vol. 272, pp. 183 - 194, 2014.

[11] J. Bestele e W. Klein-Heissling, «ASTEC V0 CPA module Containment Thermalhydraulics and Aerosol- and Fission Product Behaviour User Guidelines,» 2000.

[12] Sandia National Laboratories, «MELCOR Computer Code Manuals - Vol.1: Primer and Users' Guide Version 2.0,» 2010.

[13] L. Bosland, «ASTEC V2.0 rev2 code - IODE module: iodine and ruthenium behaviour in the

containment,» 2011.

[14] P. Chatelard, «Evolution of the integral code ASTEC V2.0-rev2 patch 1 with respect to the original V2.0-rev3 version,» Cadarache, 2013.

[15] P. Chatelard e N. Reinke, «Evolution of the integral code ASTEC V2.0-rev3 with respect to the original V2.0 version,» 2009.

[16] Sandia National Laboratories, «MELCOR Computer Code Manuals Vol. 2: Reference Manual,» 2008.